On the computations of a new interaction model between free surface flows and sediment transport

Arno Roland Ngatcha Ndengna

Finite volume AENO methods with flux time-steps discretization procedure for a averaged sediment transport model

Arno Roland Ngatcha Ndengna[a], Abdou Njifenjou[a,b], Boniface Nkonga[c]

[a] *Laboratory E3M, National High Polytechnic school of Douala, University of Douala , P.O.BOX 2107, Douala, Cameroon*
[b] *Department of Mechanical Engineering National Advanced School Polytechnic, University of Yaounde I,P.O.BOX 8390, Yaounde, Cameroon*
[c] *Université Côte d'Azur, INRIA, CNRS and LJAD, 06108 Nice Cedex 2,France*

Abstract

During Dam-breaks, the energy of the flow increases mobilizing the sediment supply and transporting it while rapidly modifying the geometry of the bottom. These observations made in natural environment leads us to develop a sediment transport model integrating all the physical and hydrodynamic processes to achieve a accurate simulation of the solutions of coastal engineering problems. Here a averaged sediment transport (ST) model is proposed to predict sediment-concentration variation and bed evolution in the shallow water flows. The model incorporate the effects of intense sediment exchange and rapid morphodynamic. Second order well-balanced preserving positivity shock capturing methods is developed for solving the proposed fully coupled ST model. The model consist to the Shallow water Generalized Equation (SWGE) taking into account density variation, sediment exchange and friction term coupled with sediment concentration equation and Exner-based equation with special approximation to compute the bed morphological process. The nonconservative system obtained is a nonlinear hyperbolic partial differential equations(PDEs). The difficulty related in determining eigenvalues and eigenvectors of fully system is avoided using the flux vector splitting technique which allowed to obtain two subsystems each having a simple eigenstructure. A special reconstruction procedure and a flux time-step algorithm are developed here to achieve second order accuracy of proposed numerical method and to guarantee the well-balanced property and the positivity of the water depth of scheme. The proposed predictor-corrector splitting method is verified on a number of numerical experiments.

Keywords: Fully coupled sediment transport model, Well-balanced preserving-positivity shock-capturing method, Flux time-step algorithm, AENO nonlinear reconstruction technique

1 Introduction

In this work, finite volume AENO methods with flux time-steps discretization procedure is developed for solving a novel one-dimensional sediment transport model. The ST model consists of: -the Shallow Water Generalized Equations were obtained by averaging over the water depth the 3D mixture sediment/fluid flows equations, -the Exner-based equation used to model the bed-load transport, -the sediment concentration equation to model the suspended load transport. The system obtained is a nonconservative equation and admits a complex eigenstructure. In this case, the upper/lower bounds on thelargest/smallest local speeds of propagation can be estimated using the Lagrange theorem(see for instance [55]). Few numerical methods for nonconservative problems designed satisfied at same time the following major properties: -well-balanced that is it exactly capable to preserves steady-state solutions (lake at rest states) even in presence of wet-dry interfaces; -it stably simulates the wet-dry zones without numerical oscillations;- it stably handles the discontinuities since the nonconservative products are well-defined.-positivity-preserving that is it capable to maintain the water depth nonnegative during the simulation without reducing the global time step. The last property ensures the robust performance of the scheme to solve the problem even in the situation where the water depth is zero or very small. Some schemes designed verified certain of these properties we cite:

(1) well-balanced schemes (see for instance [43],[48]), (2) Godunov-type path-conservative methods were originally introduced in[22] and its variants (seeforinstance[34],[20] and the references therein),(3) Central-Upwind schemes see for instance[32]),(4) Finite volume based on Riemann solver approximations or Roe solver approximations using some numerical fluxes functions (seeforinstance[1],[12],[13], [38],[42],[37]), or other solvers such that Harten, Lax and Van Leer(HLL) solver see [25] (exact Riemann solver see for instance [41]), and its variants as Harten, Lax and Van Leer with contact(HLLC) solver(see [26]), (5)splitting schemes (see for instance[45],[8]), (6) path-conservative central-upwind (PCCU)schemes (see for instance [11]).One difficulty often met in PCCU schemes is related to the numerical computation of steady-state and quasi-steady-state solutions in presence of sediment (when the bed moves). Classical HLL solver is an incomplete Riemann solver that accounts for the fastest and slowest wave speeds of propagation. One major of the Riemann HLL scheme is increasing the numerical diffusion (or dissipation). Few finite volume methods were developed for the fully coupled sediment transport models due to their complex eigenstructure. A strategy tosolve this drawback is a splitting technique. The flux splitting technique consists of dividing the fully coupled system in twosubsystems each having a simple eigenstructure. Shallow water with constant density coupled with Exner equation using a splitting method have been developed by [45] but without friction source term, suspended transport, transportation/depositionexchange and density variability. The proposed scheme is more general than that proposed by [45] integrates all the above effects. For some above schemes, the evaluation of eigenvalues and eigenvectors in the presence of a bed-load equation integrating the complex sediment flux formula and suspension equation fails.The use in this case of a splitting flux method can be interesting.This is interesting because the determination of eigenstructure becomes less difficult. Here, a splitting scheme is developed with special properties well-known in the finite volume methods.

Weuse here a path-conservative Riemann solver technique to discretize the pressure problem. The Φ-approximated HLL-Riemann solver is the building block of a finite volume method and this approach is used for the non conservative pressure subsystem described in the proposed model . A such technique has been used in some paper in literature to solve nonconservative problems(see for instance Castro et al[13], Nkonga and Praveen [41], and Bhole et al [8]). We develop in this paper a finite volume method based on path-conservative HLL Riemann solver coupled with advection scheme to address the nonconservative problem related to the proposed model.

It is well-known that the certain properties of the finite volume schemes proposed in the literature are not rigorously demonstrated. In this paper, we prove a number ofcrucial properties of our proposed second order splitting scheme such that the so-called C-property introduced by [7], the positivity of water depth, which impacts directly or indirectly the stability of FVS scheme. The generation of negative water heights during the simulation can lead to a loss of stability of our numerical scheme.This positivity is obtained by using appropriate procedures described in this paper. The numerical scheme developed and presented here can treat the discontinuities and capture shocks associated with Dam-break on erodible or non erodible beds.

The dry area is treated with a novel technique proposed here. To achieve second-order accuracy in space and time, AENO (Averaging Essentially non oscillatory) reconstruction and semi-implicit Runge-Kutta method with flux time-steps are used. The obtained second order scheme is interesting and can be interpreted as a predictor-corrector.

One of the purposes of this paper is to show that the finite volume splitting scheme developed here accommodates very well to general nonlinear hyperbolic nonconservative total sediment transport equations. It also shows that the scheme reproduces well-known classical path-conservative, HLL Riemann solver, etc. Another goal here would be to demonstrate the numerical performance of our method on various problems existing in literature. The rest of the paper is organized as follows. In section 2, we rewrite the model in different form and we propose several properties of the system. In section 3, we present a notion of path-conservative solution and Rankine-Hugoniot (R-H) relation for our model. In section 5, we present some approximations for both sub-systems. In section 5, we present first order FVS scheme and second order extension in space of FVS scheme by a modified AENO reconstruction. Well-balanced property discretization source terms are also presented.

In Section 6, we present well-balanced property and preservation positivity of water height of proposed method. Some new results are proven.

In section 7, we develop a semi-implicit Runge-Kutta AENO method with flux time-steps to achieve the

second order fully discrete FVS scheme.

In Section 8, we present several numerical examples demonstrating a superb performance of the proposed splitting scheme. We conclude in Section 9.

2 Mathematical modelings

The starting point is to consider that the motions of each phase (sediment and fluid) are governed by two conservation equations of mass and momentum. The approach here does not consist in solving for each phase the equations but to write an equation of conservation of momentum for the mixture. By summing on two phases the equations of each phase we find a mixed horizontal flow (fluid of variable characteristics) model.

The various equations that go with it, their mathematical formulation and the associated closure relations are presented. Then we will give some useful properties of our developed model and make a spectral analysis of the model.

2.1 Constitutive relations and closure formulas

The sediment transport model developed here is obtained by coupling the Shallow Water Equations (SWE) with density variation(also called Shallow Water Generalized Equations), the bed evolution equation and the sediment concentration equation.

Shallow Water Generalized Equations.

SWE is a hyperbolic equation of first-order Partial Differential Equations (PDE) are made up of conservation laws of mass and momentum in fluid mechanics. The generalized Shallow Water Equations are obtained by averaging 3D mixture flows taking into account the density variation of water due to the presence of sediment. These equations read:

$$\begin{cases} \dfrac{\partial h}{\partial t} + \dfrac{\partial hu}{\partial x} = \dfrac{(E-D)}{(1-p)} \\ \dfrac{\partial hu}{\partial t} + \dfrac{\partial}{\partial x}\left(huu + \dfrac{1}{2}gh^2\right) = S_F - gh\dfrac{\partial b}{\partial x} - \dfrac{\delta\rho}{2\rho}gh^2\dfrac{\partial C}{\partial x} - \dfrac{(E-D)u}{(1-p)} \end{cases} \tag{1}$$

The first equation of the system (1) is the fluid mass conservation, the second equation is the fluid momentum conservation which integrates the deposition/entrainment exchange.

In system (1), $u[m/s]$ is the vertically-averaged velocity components; $h = h(\mathbf{x}, t)[m]$ is the water depth. C is the flux-averaged volumetric sediment concentration (m^3/m^3); $x[m]$ is the streamwise coordinate and g is the gravitational acceleration (m/s^2); $b[m]$ is bed morphology; $w = h + b$ is the free surface; p is the bed porosity, ρ_w, ρ_s, ρ are respectively the density of water, density sediment and water-sediment mixture density which is given by:

$$\rho = \rho_w(1 - C) + \rho_s C. \tag{2}$$

$S_F = -ghS_f$ is the friction source term, which depends on the flow condition. When the flow is laminar, Manning's friction law is often used:

$$S_f = n^2 h^{-10/3}|q(h,u)|q(h,u) \tag{3}$$

where n is Manning's roughness coefficient.

The Manning coefficient n depends on the characteristic amplitude and spatial scales (l) of the irregular structure of the mobile bed b. The Manning coefficient should be defined following a wide range of scales of bed inhomogeneities For the small-scale inhomogeneities $(l < 50m)$ with the amplitude $\Delta b < 0.8$ we can take $n = 0.0025$. For the large-scale inhomogeneities n does not exceed 0.02 [17].

E and D represent the rate of transportation and deposition. We have put $\delta\rho = (\rho_s - \rho_w)$. The nonconservative term $\dfrac{(\rho_s - \rho_w)}{2\rho}gh^2\dfrac{\partial C}{\partial x}$ present in (1) contains a power of h. It would be more elegant to write in the following form:

$$\frac{\delta\rho}{2\rho}gh^2\frac{\partial C}{\partial x} = \frac{\delta\rho}{2\rho}g\left(h\frac{\partial hC}{\partial x} - hC\frac{\partial h}{\partial x}\right). \tag{4}$$

Bed evolution and sediment concentration equations

The sediment concentration equation and bed evolution equation are modeled based on the mass and momentum conservation of sediment water-sediment mixture. These equations are:

$$\frac{\partial hC}{\partial t} + \frac{\partial}{\partial x}\left(hF_{cor}uC\right) = \frac{\partial}{\partial x}\left(h\mathbf{D}_x\frac{\partial C}{\partial x}\right)$$
$$\frac{\partial b}{\partial t} + \mu\frac{\partial \widetilde{q}_b}{\partial x} = -\frac{(E-D)}{1-p}$$

In Eq.(5a), $\mu = \dfrac{A_g}{1-p}$, where A_g is a coefficient usually obtained experimentally by taking into account the grain diameter and the kinematic viscosity of the sediment mixture. In the considered context, the sediment transport flux is computed using the energetic-based formula of [2] where small values proportional to the bottom slope are neglected. In Eq.(5a), $\widetilde{q}_b$ given by

$$\widetilde{q}_b = u^3, \tag{6}$$

is the approximation of depth-average of the horizontal speed to the cubic power[55].

In equation(5a), $\mathbf{D}_x$ is the viscosity coefficient. Assuming that the suspension is sufficiently dilute (Boussinesq approximation) we can consider that the value of the kinematic viscosity is equals to the corresponding to clear water. F_{cor} represents the correction of averaged-velocity u [29]:

$$F_{cor} = \frac{I_2 - \log(B/30)I_1}{I_1\log(eB/30)}, \tag{7}$$

where I_1, I_2 are given by [16]:

$$I_1 = \begin{cases} \dfrac{1}{1-R}(1-B^{1-R}), R \neq 1 \\ -\log(B), R = 1 \end{cases} \quad , \quad \text{and} \quad I_2 = \begin{cases} \dfrac{I_1 + \log(B)B^{1-R})}{R-1}, R \neq 1 \\ -0.5(\log(B))^2, R = 1, \end{cases}$$

where $B = \dfrac{h}{k_s}$ with k_s is a roughness coefficient (given bellow) and where R the Rouse number given by: $R = \dfrac{W_s}{\kappa u_*}$ used to define the mode of sediment transport: bedload or suspension. E and D represent the entrainment and deposition terms determined by assuming that the sediments are non-cohesive. We use empirical relations for E and D taking into account sediment supply conditions and longitudinal slope of bed. Following [9],[24],[52], we have:

$$E = \begin{cases} \phi(\theta - \theta_{cr}(\alpha))\dfrac{1}{h}|u|d_{50}^{-0.2} & \text{if}\theta \geq \theta_{cr}(\alpha) \\ 0 \quad \text{Otherwise} \end{cases} \quad , \qquad D = W_s(1-C_a)^m C_a \tag{8}$$

For sediment deposition, the sediment fall velocity is given by $W_s = \sqrt{(\dfrac{13.95\nu}{d})^2 + 1.09sgd} - 13.95\dfrac{\nu}{d}$, where $\nu = 1.2\times10^{-6}$. m indicates the effects of hindered setting due to high sediment concentration. C_a is the local near-bed sediment concentration in volume, which can be determined by [9]:

$$C_a = \alpha_c C, \tag{9}$$

where α_c is given by[28]:

$$\frac{1}{\alpha_c} = \begin{cases} \left|\dfrac{A(1-A^r)}{r}\right| & \text{if } |R-1| > 10^{-4} \\ |-A\log(A)| & \text{if } |R-1| < 10^{-4} \end{cases} \tag{10}$$

and where

$$r = \begin{cases} \min(R-1,3) & \text{if } |R-1| > 10^{-4}, \\ 0 & \text{if } |R-1| < 10^{-4}, \end{cases} \tag{11}$$

where $A = \max(\frac{\delta_a}{h}, 1)$, δ_a the height of the bedload zone. For sediment entrainment E, φ is the coefficient which control the erosion forces, $\theta_{cr} = 0.55$ is the critical value of Shields parameter motion.

θ^* is the modified Shields parameter defined by

$$\theta^* = \frac{\Psi u_*}{g\cos(\alpha) s d_{eff}} \tag{12}$$

where u_* is the function velocity defined using the manning coefficient $u_* = \sqrt{C_f u^2}$ and where d_{eff} is the effective diameter of sediment taking into account shape of grain. $d_{eff} = \frac{d_{50}}{\sqrt{C_{50}}}$ where C_{50} is circularity index of grain. Ψ is the skin friction correction given by:

$$\Psi = \frac{2\kappa^2}{C_h[\log(\frac{11.036h}{k_s})]^2} \tag{13}$$

where C_h is the Nikuradse quadratic drag coefficient given by:

$$C_h = \frac{2\kappa^2}{\log(441.44h)^2}. \tag{14}$$

Here, κ is the von Karman number. k_s is a roughness coefficient (m) which accounts the sediment condition supply. Note that the amount of sediment that can be moving on a sedimentary bedforms or sediment supply is not negligible on the bed morphodynamic. The sediment supply condition impacts the sediment transport in coastal context and plays a role on deposition/transportation processes. The impact of the sediment supply condition on the morpodynamics of bedform subjects to a current was experimentally studied in coastal context by Vah et al [49]. We have [50]:

$$k_s = 3d_{90} + 1.1h_{eq}(1 - \exp\left(\frac{-25h_{eq}}{\lambda_{eq}}\right), \tag{15}$$

Here, $d_{90}(m)$ is the representative grain size in which 90% of all particles in the bed are smaller. $h_{eq}(m)$ is the equivalent height, $\lambda_{eq}(m)$ is the bed form length. Taking account supply conditions, we have:

$$\frac{\lambda_{eq}}{\lambda_{eq_i nf}} = 1 - \beta_T \exp\left(\frac{-\delta}{\gamma_T h_{eq_i nf}}\right). \tag{16}$$

A best results are obtained when $\beta_T = 0.48$, $\gamma_T = 0.62$ (however, more data are needed to confirm the coefficients adjustments in the case of ripples [49])

$$\frac{h_{eq}}{h_{eq_i nf}} = 1 - \beta_T \exp\left(\frac{-\delta}{\alpha_T \theta' h_{eq_i nf}}\right) \tag{17}$$

$\alpha_T = 8.24$. θ' is the Shields parameter calculated without bedforms or skin friction Shields parameter and is given by

$\theta' = \frac{u'_*}{(s-1)gd_{50}}$ with u'_* bottom velocity without bedforms and based on grain diameters.

$h_{eq_i nf}$ and $\lambda_{eq_i nf}$ are respectively the height and length at the equilibrium state for unlimited sediment supply conditions $[m]$ defined following [**?**]:

$$h_{eq_i nf} = 202 d_{50} D_*^{-0.554}, \quad \lambda_{eq_i nf} = d_{50}\left(500 + 1881 D_*^{-1.5}\right) \tag{18}$$

To obtain a well-posed problem we add to (1), (5a) some initial conditions $h(x,0) = h_0(x)$, $q(x,0) = q_0(x)$, $(hC)(x,0) = (hC)_0(x)$, $b(x,0) = b_0(x)$ and boundary conditions.

2.2 Eigenproblem of the total load sediment transport model

Eq.(1) and Eq.(5a) written in vector form as:

$$\begin{cases} \dfrac{\partial W}{\partial t} + \dfrac{\partial F(W)}{\partial x} = S_0(W) + S_c(W) + S_e(W) + S_F(W); \quad x \in \Omega \subset \mathbb{R}, t \in (0,T) \\ W(x,0) = W_0, \\ \text{Boundaries conditions.} \end{cases} \tag{19}$$

where $\dfrac{\partial F(W)}{\partial x}$ is the conservative term, $W = \begin{pmatrix} h \\ q \\ hC \\ b \end{pmatrix}$ and $F(W) = \begin{pmatrix} hu \\ huu + \dfrac{1}{2}gh^2 \\ F_{cor}huC \\ \dfrac{A_g}{1-p}u^3 \end{pmatrix}$.

S_0, S_f, S_c, S_e in (19) are the source terms respectively topography source term, friction source term and sediment/fluid exchange source terms. These terms are:

$$S_0 = \begin{pmatrix} 0 \\ -gh\dfrac{\partial b}{\partial x} \\ 0 \\ 0 \end{pmatrix}, \quad S_c = \begin{pmatrix} 0 \\ -\dfrac{\delta\rho}{2\rho}gh^2\dfrac{\partial C}{\partial x} \\ 0 \\ 0 \end{pmatrix}, \quad S_F = \begin{pmatrix} 0 \\ -ghS_f \\ \dfrac{\partial}{\partial x}\left(h\mathbf{D}_x\dfrac{\partial C}{\partial x}\right) \\ 0 \end{pmatrix}, \quad S_e = \begin{pmatrix} \dfrac{E-D}{1-p} \\ -\dfrac{(E-D)u}{(1-p)} \\ E-D \\ -\dfrac{E-D}{1-p} \end{pmatrix}.$$

$W = W(x,t) \in \mathcal{C} \subset \mathbb{R}^{N_\lambda}$ is the vector containing the conserved variables that takes values on $\mathcal{C}$, with the number of equations N_λ.

$F(W) : \mathcal{C} \to \mathbb{R}^{N_\lambda}$ is the physical fluxes on the x-direction. By using the Jacobian matrix $\dfrac{\partial F(W)}{\partial W}$, the Eq.(19) can be rearranged in non-conservative form as:

$$\frac{\partial W}{\partial t} + \mathcal{A}(W)\frac{\partial F(W)}{\partial W} = \widehat{S}(W), \quad W \in \mathcal{C} \subseteq \mathbb{R}^{N_\lambda} \tag{20}$$

where $\widehat{S}(W) = S_e + S_F$ and where $\mathcal{A}(W) = \dfrac{\partial F(W)}{\partial W} + B(W) + C(W)$. that is:

$$\mathcal{A}(W) = \begin{bmatrix} 0 & 1 & 0 & 0 \\ -u^2 + gh - \dfrac{\delta\rho ghC}{2\rho} & 2u & 0 & gh \\ F_{cor}uC & F_{cor}C & F_{cor}u & 0 \\ \dfrac{-3A_g u^3}{h} & \dfrac{3A_g u^2}{h} & 0 & 0 \end{bmatrix}$$

Eq.(20) provides sufficient information for the hyperbolicity of the system. The system (20) is said to be hyperbolic if the matrix $\mathcal{A}(W)$ admits N_λ distinct reals values, then the system is said strictly hyperbolic. With a such eigenvalues, we define the eigenvectors associated $E_1(W), E_2(W), ..., E_{N_\lambda}(W)$ therefore it is possible define ones matrix $P = (E_m)_{1 \le m \le N_\lambda}$ and $P^{-1}(W)$ with the diagonalization property, the Jacobian can be rewritten :

$$\mathcal{A}(W) = P(W)\Lambda(W)P^{-1}(W) \tag{21}$$

$\Lambda(W) = diag(\lambda^1(W), ..., \lambda^{N_\lambda}(W))$ a diagonal matrix composed by the eigenvalues of the Jacobian. The system is supposed to be strictly hyperbolic and the characteristic fields E_i, $i = 1, ..., N_\lambda$ are supposed to be either genuinely nonlinear:

$\nabla\lambda_i(W).E_i(W) \neq 0, \nabla W \in \Omega$ or linearly degenerate:

$\nabla\lambda_i(W).E_i(W) = 0, \nabla W \in \Omega.$

The characteristic polynomial of the coefficients matrix $\mathcal{A}$ is obtained by setting $\det(\mathcal{A} - \lambda I) = 0$ where I is the 4×4 identity matrix. The Jacobian matrix associated with the conservative flux $F(W)$ is diagonalizable

(Hyperbolic system). When adding the nonconservative contribution associated with the derivative of b, hC and h the hyperbolicity of the left-hand side (LHS) is no longer guaranteed. This will lead to further numerical complications. However, when the sediment flux is removed into an Exner-based equation, we find a model similar to that developed by [9] and the system Eq.(20) is of the hyperbolic type being real and distinct of the four eigenvalues of the matrix $\mathcal{A}$:

$$\lambda_1 = 0, \quad \lambda_2 = F_{cor}u, \quad \lambda_{3,4} = u \pm \sqrt{gh + (1 - F_{cor})\frac{\delta\rho ghC}{2\rho}}. \tag{22}$$

when $F_{cor} = 1$ we find easily the eigenvalues proposed by [4].

The third and fourth eigenvalues correspond to genuinely non-linear characteristic fields in the sense of Lax [33]. While remaining eigenvalues correspond to linearly degenerate characteristic fields. $\lambda_{3,4}$ are associated with shock rarefaction. Riemann invariants are constant across linearly degenerate waves and rarefaction waves whereas for shock waves generalized jump conditions should be satisfied.

Remark 2.1. *For two-dimensional case developed by [55], a computationally expensive process of finding all of the eigenvalues of the Jacobian matrices has been avoided: The upper/lower bounds on the largest/smallest local speeds of propagation are estimated using the Lagrange theorem. Here, using a splitting technique we compute easily the upper/lower bounds on the largest/smallest local speeds of propagation without using Lagrange or Gerschgorin theorems.*

2.3 A splitting technique for our model.

Originally the splitting technique was applied for the Euler equations by[47] and recently for a rather simple Saint-Venant-Exner model (without source terms and sediment effects) by [45]. In the following, we will apply the same technique for a more general sediment transport model presented above. The splitting technique consists in separating the total flux $F(W)$ with a rather complicated eigenstructure into a sum of two others fluxes $F^{(p)}(W)$ and $F^{(a)}(W)$ called pressure and advection fluxes respectively whose Jacobian matrices associated are rather simple to analyze.

$$F(W) = \begin{pmatrix} q \\ \left(\frac{q^2}{h} + \frac{1}{2}gh^2\right) \\ F_{cor}huC \\ \frac{A_g}{1-p}u^3 \end{pmatrix} = F^{(p)} + F^{(a)} \quad \text{where} \quad F^{(p)} = \begin{pmatrix} hu \\ \frac{1}{2}gh^2 \\ F_{cor}huC \\ 0 \end{pmatrix}, \quad F^{(a)} = \begin{pmatrix} 0 \\ hu^2 \\ 0 \\ \frac{A_g}{1-p}u^3 \end{pmatrix} = q\begin{pmatrix} 0 \\ q/h \\ 0 \\ \frac{A_g}{1-p}u^2/h \end{pmatrix} \tag{23}$$

Therefore, the two subsystems obtained are given by:

$$\begin{cases} \dfrac{\partial W}{\partial t} + \dfrac{\partial F^{(p)}(W)}{\partial x} + B(W)\partial_x W + C(W)\partial_x W = 0; \\ \dfrac{\partial W}{\partial t} + \dfrac{\partial F^{(a)}}{\partial x} = \widehat{S}(W); \end{cases} \tag{24}$$

and are named pressure subsystem and advection subsystem respectively. The pressure system is non-conservative and the advection subsystem is conservative.

In next we will solve each subsystem by different numerical techniques well known in literature. The pressure conservative system is resolved by simple Riemann solver based on approximation Riemann solver. The advection system is solved by using a advection method.

2.4 Simple eigenstructure for pressure and advection systems: approximation of the wave velocities.

Let us recall that for stability reason the eigenvalues of the each subsystem must be upper bounds of the eigenvalues of the Jacobian matrix $\mathcal{A}^{(m)}$, $m = p, a$ of the each subsystem.

2.4.1 Simple eigenstructure for pressure subsystem

The pressure subsystem is nonconservative because the momentum equation of (1) contains two nonconservative terms $g\frac{\delta\rho}{2\rho}\left[h\frac{\partial hC}{\partial x} - hC\frac{\partial h}{\partial x}\right]$, and $gh\frac{\partial b}{\partial x}$. We can rewrite the pressure system as:

$$\frac{\partial W}{\partial t} + \mathcal{A}^{(p)}(W)\frac{\partial W}{\partial x} = 0; \tag{25}$$

where $\mathcal{A}^{(p)}(W) = \frac{\partial F^{(p)}(W)}{\partial W} + B(W) + C(W)$ and where $C(W) = \begin{bmatrix} 0 & 0 & 0 & 0 \\ -\frac{\delta\rho ghC}{2\rho} & 0 & \frac{\delta\rho gh}{2\rho} & 0 \\ 0 & 0 & 0 & 0 \\ 0 & 0 & 0 & 0 \end{bmatrix}$ and $B(W) = \begin{bmatrix} 0 & 0 & 0 & 0 \\ 0 & 0 & 0 & gh \\ 0 & 0 & 0 & 0 \\ 0 & 0 & 0 & 0 \end{bmatrix}$.

That is:

$$\mathcal{A}^{(p)} = \begin{bmatrix} 0 & 1 & 0 & 0 \\ gh - \frac{\delta\rho ghC}{2\rho} & 0 & \frac{\delta\rho gh}{2\rho} & gh \\ -F_{cor}uC & F_{cor}c & F_{cor}u & 0 \\ 0 & 0 & 0 & 0 \end{bmatrix} \tag{26}$$

The eigenvalues of Jacobian matrix $\mathcal{A}^{(p)}$ are $\lambda_1^{(p)} = -\sqrt{gh - (1 - F_{cor})\frac{\delta\rho ghC}{2\rho}}, \lambda_2^{(p)} = 0, \lambda_3^{(p)} = F_{cor}u, \lambda_4^{(p)} = \sqrt{gh - (1 - F_{cor})\frac{\delta\rho ghC}{2\rho}}$.

We have well $\lambda_1^{(p)} < \lambda_2^{(p)} < \lambda_3^{(p)} < \lambda_4^{(p)}$
where $\lambda_1^{(p)}$ and $\lambda_4^{(p)}$ are the upper bounds of Jacobian matrix $\mathcal{A}^{(p)}$ flux of pressure system.

2.4.2 Simple eigenstructure for advection subsystem

We recall that the advection subsystem is given by:

$$\frac{\partial W}{\partial t} + \frac{\partial F^{(a)}}{\partial x} = \widehat{S}(W); \tag{27}$$

where $W = (h, hu, hC, b)^t$ and $F^{(a)}$ as in (23).

The quasi-linear form is form by:

$$\frac{\partial W}{\partial t} + \mathcal{A}^{(a)}\frac{\partial W}{\partial x} = \widehat{S}(W); \tag{28}$$

The Jacobien matrix for advection system is given by:

$$\mathcal{A}^{(a)} = \frac{\partial F^{(a)}}{\partial W} = \begin{bmatrix} 0 & 0 & 0 & 0 \\ -u^2 & 2u & 0 & 0 \\ 0 & 0 & 0 & 0 \\ \frac{-3A_g u^3}{h} & \frac{3A_g u^2}{h} & 0 & 0 \end{bmatrix}.$$

A simple calculation give the following eigenvalues:

$\lambda_1^{(a)} = \lambda_2^{(a)} = 0, \quad \lambda_3^{(a)} = \lambda_4^{(a)} = 2\alpha u.$

We shows that $\lambda_{1,2}^{(a)}-$field is linearly degenerate since $\nabla_W \lambda_1^{(a)}.E_1^{(a)}=0$, while the $\lambda_3^{(a)},\ \lambda_4^{(a)}$ are genuinely non linear if $u\neq 0$. In fact $\nabla_W \lambda_{3,4}^{(a)}.E_4^{(a)}\neq 0$. The advection system is weakly hyperbolic. Its proven that the weakly hyperbolic nature of the advection system does not impact its numerical approximation (see numerical tests bellow).

3 Notion of path-conservative solution and Rankine-Hugoniot relation

3.1 Notion of path-conservative solution

The non-conservative terms present in (1) can be viewed as Borel measure [18]. This definition required the choice of sufficiently smooth paths $\Psi(s)=\Psi(s,W_L,W_R)$ connecting the two states $W_L\ W_R$ across the jump discontinuity at $\mathbf{x}=\mathbf{x}_0$ such that a local-Lipschitz application $\Phi:[01]\times\Omega\times\Omega\to\Omega$ satisfies the following property:

$$\Psi(0,W_L,W_R)=W_L \ \text{ and } \ \Psi(1,W_L,W_R)=W_R, \ \text{ for all } \ W_L,W_R\in\Omega.$$

We can defined the nonconservative product as the Borel measure [18]:

$$\mu(\mathbf{x}_0)=\left[\int_0^1 \mathcal{A}(\Phi(s,W_L,W_R))\frac{d\Phi}{ds}(s,W_L,W_R)ds\right]\delta(x_0),$$

where δ is the Dirac function and where $\delta(x_0)$ is the fluctuation. This definition is similar to the one proposed by Volpert [51] to define the non-conservative product.

We take a particular example of the simplest linear segment path:

$$\Psi(s,W_L,W_R)=W_L+s(W_R-W_L), \ \ s\in[01]. \tag{29}$$

The details of the theory can be found in [18] we will not insist on it.

Remark 3.1. *Note that the path-conservative notion can serve to develop a theory of weak solutions based on which the Riemann problem is usual structure as for conservative systems, leading to shocks or rarefaction waves corresponding to genuinely non-linear characteristic fields and contact waves corresponding to linearly degenerate fields. Across a point of discontinuity moving with speed σ, a weak solution has to satisfy the generalized Rankine-Hugoniot jump condition is presented in the next subsection.*

3.2 Rankine-Hugoniot relation, shock waves, Hugoniot curve.

Let us define the average and jump operators by: the average and jump operators $\{\{.\}\}$ and $[|.|]$ respectively by $[|.|]=()_R-()_L$, $\{\{.\}\}=\dfrac{()_R+()_L}{2}$ which is nothing but the arithmetic mean value. Let us only note that the weak solutions correspond to the classical solutions where they are smooth, while through a discontinuity the following generalized Rankine-Hugoniot condition must be satisfied:

$$\sigma[|W|]=\int_0^1 \mathcal{A}(\Phi(s,W_L,W_R))\frac{d\Phi}{ds}(s,W_L,W_R)ds. \tag{30}$$

For our proposed model, that is:

$$\begin{aligned}
[|hu|] &= \sigma[|h|], \\
[|\frac{q^2}{h} &+ \frac{1}{2}gh^2|]+\int_0^1 g(\Phi_h(s,W_L,W_R))\frac{d\Phi_b}{ds}(s,W_L,W_R)ds \\
&+ \int_0^1 \frac{\delta\rho}{2\rho}g\left(\Phi_h(s,W_L,W_R)\frac{d\Phi_{hC}}{ds}(s,W_L,W_R)ds-\Phi_{hC}\frac{d\Phi_h}{ds}(s,W_L,W_R)\right) \\
&= \sigma[|hu|], \\
[|F_{cor}huC|] &= \sigma[|hC|], \\
[|\mu u^3|] &= \sigma[|b|],
\end{aligned} \tag{31}$$

where Φ_h, Φ_b, Φ_{hC} are the first, third and fourth components of Φ respectively.

For the particular choice of the family of segments $\Phi(s, W_L, W_R) = W_L + s(W_R - W_L)$, the R-H relations given by (31) rewrites:

$$\begin{aligned} [|hu|] &= \sigma[|h|] \\ [|hu^2 + \frac{1}{2}gh^2|] + g\{\{h\}\}[|b|] + g\frac{\rho_s - \rho_w}{2\rho}\left[\{\{h\}\}[|hC|] - \{\{hC\}\}[|h|]\right] &= \sigma[|hu|] \\ [|F_{cor}huC|] &= \sigma[|hC|] \\ [|\mu u^3|] &= \sigma[|b|] \end{aligned} \tag{32}$$

Here, σ is a speed at discontinuity which must be zero for the Rakine-Hugionot condition to be verified.

Note that the condition of the jumps depends on the path family chosen. Therefore, their choice must guarantee a good agreement between the propagation speed of the discontinuities and physics of the problem. The calculation of this family requires the knowledge of the Riemann solutions. In practice, the family of paths is chosen so that the condition of jumps coincides with those given by the progressives waves of the regularity problems at the time of the passage to the limit. The choice made here is a family composed by the segments. This type of family is linear but other types of (non-linear) families exists (see for instance[6]) and are not considered in this work.

Remark 3.2. *A discontinuity verifies the Rakine-Hugionot relations and to be admissible must additionally verify the Lax condition. If $\sigma$is the shock speed, we have $\lambda_1^{(p)} > \sigma > \lambda_3^{(p)}$ from which we obtain two Lax inequalities$\lambda_1^{(p)} - \sigma > 0$ and $\lambda_3^{(p)} - \sigma < 0$.*
The first inequality shows that the left state is the pre-shock state since the velocity relative to the shock is positive. The second inequality conceives the possibility of connecting a state(h, hu, hC, b) to the left of a state $(h_R, (hu)_R, (hC)_R, b_R)$ by a 3-shock. Increasing the amplitude of the shocks can lead to a significant difference between the exact and numerical results.Some schemes may become unstable for large shock amplitudes.

4 Approximation for the subsystems

In this section, we present the approximation for both subsystems obtained by the splitting technique. HLL-Riemann solver is used to solve the pressure subsystem and a simple advection scheme is developed for the advection system.

4.1 Approximation by a Riemann solver of the pressure subsystem.

We recall that the pressure system is given:

$$\frac{\partial W}{\partial t} + \mathcal{A}^{(p)}(W)\frac{\partial W}{\partial x} = 0, \tag{33}$$

where $\mathcal{A}^{(p)}(W) = \dfrac{\partial F^{(p)}}{\partial W} + B^{(p)}(W) + C^{(p)}(W)$, $B^{(p)}(W) = B(W)$, $C^{(p)}(W) = C(W)$.

This system admits discontinuous solution.

Concept of family of paths

Définition 4.1. *A family of paths in $\Omega \subset \mathbb{R}^N$ is a local-Lipschitz application $\Phi : [0\ 1] \times \Omega \times \Omega \to \Omega$ that satisfies the following properties*

1. $\Phi(0, W_L, W_R) = W_L$ *and* $\Phi(0, W_L, W_R) = W_R$, *for all* $W_L, W_R \in \Omega$
2. *For a bounded set* $\Phi(s, W_L, W_R, \nu) = \Phi(1 - s, W_L, W_R, -\nu)$, *for all* $W_L, W_R \in \Omega, s \in [01]$

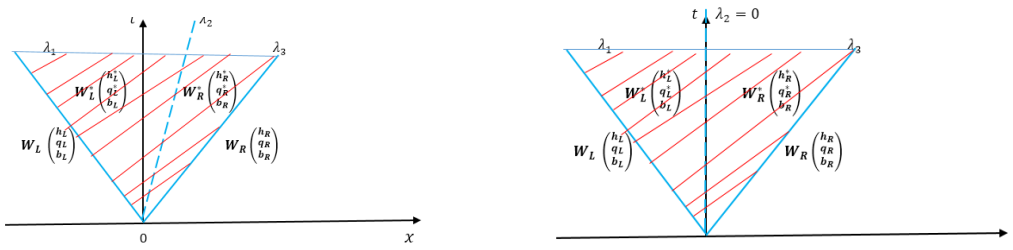

Figure 1: Wave structure in HLL-Riemann solvers. (a) $\lambda_2 > 0$, (b) $\lambda_2 = 0$

3. *For a bounded set* $\mathcal{O} \subset \Omega$ *there exists a constant* C *such that* $\left|\dfrac{\partial \Phi(s, W_L, W_R)}{\partial s}\right| \leq C|W_L - W_R|$, *for all* $W_L, W_R \in \mathcal{O}$ *and for almost all* $s \in [01]$.
4. *For a given bounded set* $\mathcal{O} \subset \Omega$, *there exist a constant* C *such that:*

$$\left|\frac{\partial \Phi(s, W_l^L, W_R^2)}{\partial s} + \frac{\partial \Phi(s, W_L^1, W_R^2)}{\partial s}\right| \leq C(|W_L^1 - W_R^2| + |W_L^1 - W_R^2|) \text{ for all } W_L^1, W_R^1, W_L^2, W_R^2 \in \mathcal{O} \text{ and}$$

for almost all $s \in [01]$.

Let us suppose that a family of paths Φ has been chosen. Based on a family paths Φ, Φ-approximate Riemann Solver for (33) is a generalization of the definition of approximate Riemann solver for system of conservation laws. We will start by assuming that the curve $\Gamma_t^x = \left\{(x,t) \in \mathbb{R} \times \mathbb{R}_+^*, x = \sigma(t)\right\}$ with $\sigma \in C^1(\mathbb{R}_+)$ satisfies Eq.(31).

Γ_t^x partitions an open domain $\Omega \subset \mathbb{R}^d \times \mathbb{R}_+$ into 4 sub-domains Ω_L,Ω_R, Ω_L^* and Ω_R^* given by:

$$\begin{aligned}
\Omega_L &= \{(x,t) \in \Omega, \Gamma_t^x < \lambda_L\}, \\
\Omega_R &= \{(x,t) \in \Omega, \Gamma_t^x > \lambda_R\}, \\
\Omega_L^* &= \{(x,t) \in \Omega, \lambda_L < \Gamma_t^x < 0\}, \\
\Omega_R^* &= \{(x,t) \in \Omega, 0 < \Gamma_t^x < \lambda_R\},
\end{aligned} \tag{34}$$

where λ_L, λ_R are characteristic velocities given by:

$$\lambda_L = \min(-c_L, -c_R, 0) \text{ and } \lambda_R = \max(c_L, c_R, 0). \tag{35}$$

Notice that any Φ-approximate Riemann solver should satisfy:

$$\int_0^1 \mathcal{A}^{(p)}\Phi(s, W_L, W_R))\frac{d\Phi}{ds}(s, W_L, W_R)ds + \int_{-\infty}^0 (\mathcal{W}_{\mathcal{R}}(\Gamma_t^x, W_L, W_R) - W_L) + \int_0^{\infty} (\mathcal{W}_{\mathcal{R}}(\Gamma_t^x, W_L, W_R) - W_R) = 0 \tag{36}$$

for every $W_L, W_R \in \Omega$. In a simple way, for the case of a Φ-approximated HLL-Riemann solver, we have:

$$\lambda_L(W_L^* - W_L) + \lambda_R(W_R - W_R^*) = \int_0^1 \mathcal{A}^{(p)}(\Phi(s, W_L, W_R))\frac{d\Phi}{ds}(s, W_L, W_R)ds \tag{37}$$

since

$$\int_0^1 \mathcal{A}^{(p)}(\Phi(s, W_L, W_R))\frac{d\Phi}{ds}(s, W_L, W_R)ds = F^{(p)}(W_R) - F^{(p)}(W_L) + \mathcal{B}(W_L, W_R) + \mathcal{C}(W_L, W_R) \tag{38}$$

where we have:

$$\mathcal{B}(W_L,W_R) = \begin{pmatrix} 0 \\ \int_0^1 g(\Phi_h(s,W_L,W_R))\dfrac{d\Phi_b}{ds}(s,W_L,W_R)ds \\ 0 \\ 0 \end{pmatrix} \text{ and} \tag{39}$$

$$\mathcal{C}(W_L,W_R) = \begin{pmatrix} 0 \\ \int_0^1 \dfrac{\delta\rho}{2\rho} g\left(\Phi_h(s,W_L,W_R)\dfrac{d\Phi_{hC}}{ds}(s,W_L,W_R)ds - \Phi_{hC}\dfrac{d\Phi_h}{ds}\right) \\ 0 \\ 0 \end{pmatrix}$$

Using the family of segments, we have:

$$\mathcal{B}(W_L,W_R) = \begin{pmatrix} 0 \\ g\{\{h\}\}[|b|] \\ 0 \\ 0 \end{pmatrix}, \mathcal{C}(W_L,W_R) = \begin{pmatrix} 0 \\ \dfrac{\delta\rho}{2\rho} g\left(\{\{h\}\}[|hC|] - \{\{hC\}\}[|h|]\right) \\ 0 \\ 0 \end{pmatrix} \tag{40}$$

If we assume that the fixe topography denoted by Z is not flat. i.e. $\dfrac{\partial Z}{\partial x} \neq 0$. The HLL-Riemann solver is slight modified to solve the pressure system. A new wave of speed is added and new variable Z takes values Z_L and Z_R for $x<0$ and $x>0$ respectively. In the system (50), only the 5th equation change and becomes:

$$\lambda_L(h_L^*u_L^* - h_Lu_L) + \lambda_R(h_Ru_R - h_R^*u_R^*) = F_R^{(2)} - F_L^{(2)} + \mathcal{B}^{(2)}\left(\mathbf{W}_L,\mathbf{W}_R\right) + \mathcal{C}^{(2)}\left(\mathbf{W}_L,\mathbf{W}_R\right), \tag{41}$$

Here, $\mathbf{W} = (W, Z)$.

$$\mathcal{B}^{(2)}\left(\mathbf{W}_L,\mathbf{W}_R\right) = \begin{pmatrix} 0 \\ g\Phi_h\left(\partial_s\Phi_b + \partial_s\Phi_Z\right)(s,\mathbf{W}_L,\mathbf{W}_R) \\ 0 \\ 0 \end{pmatrix}$$

where Φ_h, Φ_b, Φ_Z, are the components of path $\Phi = \Phi(s,\mathbf{W}_L,\mathbf{W}_R)$ corresponding to variable h, b, Z respectively.

By applying Eq.(29) we obtain:

$$\mathcal{B}(\mathbf{W}_L,\mathbf{W}_R) = \begin{pmatrix} 0 \\ g\{\{h\}\}([|b|] + [|Z|]) \\ 0 \\ 0 \end{pmatrix}$$

4.2 Brief description of path-conservative scheme

The main idea in this method is to split the fluctuation for pressure sub-system into two parts corresponding to left moving and right moving waves arising in the HLL-Riemann solution, where the fluctuation $D(W_L,W_R)$ is defined by:

$$D(W_L,W_R) = \int_0^1 \mathcal{A}^{(p)}\left(\Phi(s,W_L,W_R)\right)\frac{d\Phi}{ds}(s,W_L,W_R)ds = D^-(W_L,W_R) + D^+(W_L,W_R). \tag{42}$$

Assume that there are m waves the Φ-approximate Riemann solution with $m-1$ intermediates states. Let us denote the wave speeds as $\lambda_j, j = 1,...,m$ and the intermediate state $j = 1,...,m$ with $W_0^* = W_L$ and $W_m^* = W_R$. The fluctuation splitting is given by:

$$D^{\pm}\left(W_L,W_R\right) = \sum_{j=1}^{m} \lambda_j^{\pm}\left(W_{j+1}^* - W_j^*\right), \tag{43}$$

where $\lambda^+ = \max(0,\lambda)$, $\lambda^- = \min(0,\lambda)$. The intermediate states are obtained by satisfying the Rankine-Hugoniot conditions across all the waves. The Φ-approximate Riemann solvers of different complexity based on the number of waves including in the model can be derived.

Φ-approximate Riemann solvers have been constructed by using the generalized jump conditions to address the pressure system. The Riemann solver is constituted of 4 states see Fig 1, denoted by $\mathcal{W}_{\mathcal{R}}(\Gamma_t^x, W_R, W_L)$ at each interface $i+1/2$ defined as follows:

$$\mathcal{W}_{\mathcal{R}}\left(\Gamma_t^x, W_R, W_L\right) = \begin{cases} W_L = (h_L, q_L, (hC)_L, b_L)^T, & \text{if } (x,t) \in \Omega_L \\ W_L^* = (h_L^*, q_L^*, (hC)_L^*, b_L^*)^T, & \text{if } (x,t) \in \Omega_L^* \\ W_R^* = (h_R^*, q_R^*, (hC)_R^*, b_R^*)^T, & \text{if } (x,t) \in \Omega_R^* \\ W_R = (h_R, q_R, (hC)_R, b_R)^T, & \text{if } (x,t) \in \Omega_R \end{cases} \tag{44}$$

where W_L and W_R satisfied (32).

We can write $\mathcal{W}_{\mathcal{R}} \in \mathcal{C}^1(\Omega_L)^3 \bigcup \mathcal{C}^1(\Omega_L)^3 \bigcup \mathcal{C}^1(\Omega_L)^3 \bigcup \mathcal{C}^1(\Omega_L)^3$.

Thus $\mathcal{W}_{\mathcal{R}} : \mathbb{R} \times \Omega \times \Omega \to \Omega$ can be seen as a simple Φ-approximate Riemann solver. Since we have a finite number of speeds and intermediate states. The Riemann problem is an initial value problem where the initial data is discontinuous at a single point.

The Riemann problem is to find $W(x,t)$ solution of Eq. (33), with the following initial data

$$W(x,0) = (U(x,0), hC(x,0), b(0,x))^T = \begin{cases} W_L = (U_L, (hC)_L, b_L)^T & \text{if } x < 0, \\ W_R = (U_R, (hC)_R, b_R)^T & \text{if } x > 0. \end{cases} \tag{45}$$

where $U = (h, hu)^T$.

These solutions verified also the Rakine-Hugoniot relations for pressure system above presented.
Equipped with $\mathcal{W}_{\mathcal{R}}(\Gamma_t^x, W_R, W_L)$ we determine $\overline{W}_i$ interpreted as the average of $\widetilde{W}$ (a piecewise constant approximation for all $x \in K$ of $W(x,t)$ at time $t + \Delta t$). i.e. $\overline{W}_i(t) = \frac{1}{|K|}\int_K \widetilde{W}(x,t)dx$. We We can now defined the semi-discrete formulation using the values of intermediate states $W_{i+1/2}^{R,*}$, $W_{i+1/2}^{L,*}$ as follows:

$$\frac{d\overline{W}_i}{dt} = -\frac{1}{|K|}\left[\lambda_{i+1/2^-}^L (W_{i+1/2}^{L,*} - \overline{W}_i) - \lambda_{i-1/2^+}^R (W_{i+1/2}^{R,*} - \overline{W}_i\right] \tag{46}$$

Note that these intermediate values ensure that the scheme is consistent and preserves all the steady states.

Remark 4.1. *: **Well-balanced approximate path-conservative Riemann solver**.*
Given a curve $\gamma \in \Gamma_t^x$, with stationary solution satisfying $W(x) \in \gamma, \quad \forall x$, the splitting scheme for solving the pressure subsystem (33) is well-balanced $\forall\ \gamma$.
Our path conservative type scheme based on Φ-approximated Riemann solver $\mathcal{W}_{\mathcal{R}}$ for a curve $\gamma \in \Gamma_t^x$, if and only if 4 states $W_L^*, W_L, W_R^*, W_R \in \Gamma_t^x$, the following equalities hold:

$$\int_{-\infty}^{0} \left(\mathcal{W}_{\mathcal{R}}\left(\Gamma_t^x, W_L, W_R\right) - W_L\right) = 0; \quad \int_{-\infty}^{0} \left(\mathcal{W}_{\mathcal{R}}\left(\Gamma_t^x, W_L, W_R\right) - W_R\right) = 0. \tag{47}$$

Theses two equalities are trivially satisfied if $W_R^* = W_R$, $W_L^* = W_L$. i.e. the region in which the approximate solution takes the value W_L^* or W_R^* disappears. Therefore, the approximate Riemann solver reduces to (45) so that the numerical scheme is well-balanced.

4.3 Consistency

It is necessary that the scheme be consistent in the sense of the integral with (1). We denote by $W_{\mathcal{R}}(\Gamma_t^x, W_R, W_L)$ the exact solution of the Riemann problem for (33). Imposing that:

$$\frac{1}{mes(K_i)}\int_{K_i} \mathcal{W}_{\mathcal{R}}\left(\frac{x}{\Delta t}, W_L, W_R\right) dx = \frac{1}{mes(K)}\int_{K_i} W_{\mathcal{R}}\left(\frac{x}{\Delta t}, W_L, W_R\right) dx, \tag{48}$$

which implies that the average solution of the approximate Riemann solver $\mathcal{W}_{\mathcal{R}}$ is equal to average solution of the exact solution $W_{\mathcal{R}}$ [25]. We consider here a HLL-Riemann solver for the pressure sub-system using two waves of speed λ_L and λ_R linking four states: (W_L, W_L^*, W_R, W_R^*). Considering the system defined by jump condition related to the continuity equation for the two waves speeds and the consistency condition related to the momentum equation:

$$\begin{aligned} F_R - F_L \quad &+ \quad \frac{1}{mes(K)}\frac{1}{\Delta t}\int_K\int_0^{\Delta t}\mathcal{B}\left(W_{\mathcal{R}}(\Gamma_t^x, W_R, W_L)\right)dxdt + \frac{1}{mes(K)}\frac{1}{\Delta t}\int_K\int_0^{\Delta t}\mathcal{C}\left(W_{\mathcal{R}}(\Gamma_t^x, W_R, W_L)\right)dxdt \\ &= \quad \lambda_L\frac{\Delta t}{mes(K)}(W_L - W_L^*) + \lambda_R\frac{\Delta t}{mes(K)}(W_R - W_R^*) \end{aligned} \tag{49}$$

That is:

$$\begin{cases} \lambda_L(h_L^* - h_L) = h_L^*u_L^* - h_Lu_L \\ \lambda_L(h_R - h_R^*) = h_Ru_R - h_R^*u_R^* \\ \lambda_L(h_L^*u_L^* - h_Lu_L) + \lambda_R(h_Ru_R - h_R^*u_R^*) = F_R - F_L + \mathcal{B}^{(2)}(W_L, W_R) + \mathcal{C}(2)(W_L, W_R) \\ \lambda_L(h_L^*C_L^* - h_LC_L) = h_L^*u_L^*C_L^* - h_Lu_LC_L \\ \lambda_L(h_RC_R - h_R^*C_R^*) = h_Ru_RC_R - h_R^*u_R^*C_R^* \\ \lambda_L(b_L^* - b_L) = 0 \\ \lambda_L(b_R - b_R^*) = 0 \end{cases} \tag{50}$$

where $F_R = \begin{pmatrix} h_Ru_R \\ \frac{1}{2}gh_R^2 \\ F_{coor}h_Ru_RC_R \\ 0 \end{pmatrix}$; $F_L = \begin{pmatrix} h_Lu_L \\ \frac{1}{2}gh_L^2 \\ F_{coor}h_Lu_LC_L \\ 0 \end{pmatrix}$. and where $\mathcal{B}\left(W_{\mathcal{R}}(\Gamma_t^x, W_R, W_L)\right)$ and $\mathcal{C}\left(W_{\mathcal{R}}(\Gamma_t^x, W_R, W_L)\right)$ are the Riemann approximation of B and C.

$\overline{\mathcal{B}} = \langle\mathcal{B}\rangle_i \simeq \frac{1}{|K|}\frac{1}{\Delta t}\int_K\int_0^{\Delta t}\mathcal{B}\left(W_{\mathcal{R}}(\Gamma_t^x, W_R, W_L)\right)dxdt$ and

$\overline{\mathcal{C}} = \langle\mathcal{C}\rangle_i \simeq \frac{1}{|K|}\frac{1}{\Delta t}\int_K\int_0^{\Delta t}\mathcal{C}\left(W_{\mathcal{R}}(\Gamma_t^x, W_R, W_L)\right)dxdt$ are the mean values of source terms verifying the consistency relations given by:

$$\lim_{mes(K)\to 0,\ \Delta t\to 0,\ W_L, W_R\to W}\overline{\mathcal{B}} = S_0 = \begin{pmatrix} 0 \\ -gh\frac{\partial b}{\partial x} \\ 0 \\ 0 \end{pmatrix} \tag{51}$$

$$\lim_{mes(K)\to 0,\ \Delta t\to 0,\ W_L, W_R\to W}\overline{\mathcal{C}} = S_c = \begin{pmatrix} 0 \\ \frac{\delta\rho}{2\rho}gh^2\frac{\partial C}{\partial x} \\ 0 \\ 0 \end{pmatrix} \tag{52}$$

The parameters $\overline{\mathcal{B}}$,$\overline{\mathcal{C}}$ are the consistency approximations of $\langle B\rangle_i$ and $\langle C\rangle_i$ respectively.

The subscript $[j]$ denotes the $j-th$ components of a vector and $\mathcal{B}(W_L, W_R)$, $\mathcal{C}(W_L, W_R)$ are defined by Eq.(40). It can be easily checked that all the components of the consistency condition Eq.(30) is recovered. We have 7 equations for unknowns some are required to solve Eq.(33).

To determine the intermediate water values (h_L^*, h_R^*), let us assume that $h_R \neq 0$, $h_L \neq 0$. We apply the Riemann invariants to find the solution of system (50). Across the stationary contact discontinuity with right

eigenvectors $E_1^{(p)}$, $E_2^{(p)}$, $E_3^{(p)}$. The generalized Riemann invariants are solutions of the following Ordinary Differential Equations (ODEs):

$$\begin{cases} \dfrac{dh}{-1} = \dfrac{dq}{0} \\ \dfrac{dh}{-1} = \dfrac{db}{1} \\ \dfrac{dh}{-1} = \dfrac{db}{0} \end{cases} \tag{53}$$

We find the Riemann invariants by analyzing the integrals curves of the eigenvector fields. The integral curve corresponding to satisfy the above set of equations.

After integration the first and second equation of system (53) in phase space we have respectively

$$q^* = q_R^* = h_R^* u_R^* = h_L^* u_L^* = q_L^*, \tag{54}$$

$$h_L^* - h_R^* = \Delta b^* = b_R^* - b_L^*. \tag{55}$$

The second component of the third equation implies that

$$[|b|]_L^R = [|b^*|]_L^R, \tag{56}$$

i.e. b remain constant across the left and the right wave ($b_R^* = b_R$).
Using the closure relations, the 8 unknowns $h_L^*, h_R^*, u_L^*, u_R^*, b_L^*, b_R^*, C_L^*, C_R^*$ of system (50) can be determined.

$$\begin{aligned} h_L^* &= \frac{h_L(\lambda_L - u_L)}{\lambda_L - u_L^*}, \quad h_R^* = \frac{h_R(\lambda_R - u_R)}{\lambda_R - u_R^*}, \\ u^* &= \frac{h_L u_L(\lambda_L - \alpha u_L) - h_R u_R(\lambda_R - \alpha u_R) + Q_{RL}}{h_L(\lambda_L - u_L) - h_R(\lambda_R - u_R)}, \\ u_L^* &= u^*, \quad u_R^* = u^* \\ b_R^* &= b_R, \quad b_L^* = b_L, \\ C_R^* &= C_R, \quad C_L^* = C_L, \end{aligned} \tag{57}$$

where $Q_{RL} = \dfrac{1}{2} g h_L^2 - \dfrac{1}{2} g h_R^2 + \mathcal{B}(W_L, W_R) + \mathcal{C}(W_L, W_R)$.

Remark 4.2. *We observe that:*
- *The velocities coincide at the intermediate regions $u_R^* = u_L^*$, and are equal to the intermediate velocities u^*.*
- *The variation of the sediment concentration C is associated to the wave u^*.*
- *One particularity of the HLL-solver used is the fact that $h_L^* \neq h_R^*$.*
- *We have $b_R^* = b_R, b_L^* = b_L, C_R^* = C_R, C_L^* = C_L$ i.e. C and b remain constant across the left and right wave.*

The use of Φ-simple HLL-Riemann solver allowed us to determine in the two star regions. These solutions being now known, the left fluctuation $D_{i+1/2}^+$ between W_L^* and W_{i+1}^n and the fluctuation $D_{i+1/2}^-$ between W_i^n and W_R^* can be computed:

$$\begin{aligned} D_{i+1/2}^+ &= \frac{1}{\Delta t} \int_0^{\Delta t} \int_0^1 \mathcal{A}^{(p)}(\Phi(s, W_L, W_R^*)) \frac{d\Phi}{ds}(s, W_L, W_R^*) ds, \\ D_{i+1/2}^- &= \frac{1}{\Delta t} \int_0^{\Delta t} \int_0^1 \mathcal{A}^{(p)}(\Phi(s, W_L^*, W_R)) \frac{d\Phi}{ds}(s, W_L^*, W_R) ds. \end{aligned} \tag{58}$$

We notice that the calculation of these fluctuations integrates the solutions in the two star regions in particular W_L^* and W_R^* given by Eq. (57).
In the Eq. (58) we have used:

$$\Phi(s, W_L^*, W_{i+1}) = W_L^* + s(W_{i+1} - W_L^*), \quad \Phi(s, W_i, W_R^*) = W_i + s(W_R^* - W_i) \tag{59}$$

$$\begin{aligned} D_{i+1/2}^{+} &= (\widehat{\mathcal{A}^{(p)}})_{i+1/2}^{+}[W_R - W_L^*], \quad D_{i+1/2}^{-} = (\widehat{\mathcal{A}^{(p)}})_{i+1/2}^{-}[W_R^* - W_L] \\ (\widehat{\mathcal{A}^{(p)}})_{i+1/2}^{-} &= \int_0^1 \mathcal{A}^{(p)}\Phi(s, W_L^*, W_R))ds, \quad (\widehat{\mathcal{A}^{(p)}})_{i+1/2}^{+} = \int_0^1 \mathcal{A}^{(p)}(\Phi(s, W_L, W_R^*))ds \end{aligned} \tag{60}$$

We approximate the integral by a nG-Gaussian quadrature formula. Therefore, $(\widehat{\mathcal{A}^{(p)}})_{i+1/2}^{-}$ is expressed as follows:

$$(\widehat{\mathcal{A}^{(p)}})_{i+1/2}^{-} = \sum_{j=1}^{n} G p_j \mathcal{A}^{(p)}(\Phi(s_j, W_L^*, W_R)), \tag{61}$$

where nG is the number of point Gaussian quadrature, p_j are the quadrature for the interval $[0, 1]$ such that $\sum p_j = 1$ and $s_j = \left\{ s_j^{\beta}, \beta = 1, ..., nG \right\}$ are the positions distributed in the interval $[0, 1]$. For instance $(0, s_j^{\beta})(\beta = 1, ..., nG)$ are the Gauss quadrature point on the right of 0. Since the quadrature is exact for the polynomial of degree $2k - 2$, we have:

$$(\widehat{\mathcal{A}^{(p)}})_{i+1/2}^{-} = \sum_{j=2}^{nG-1} p_j \mathcal{A}^{(p)}(\Phi(s_j, W_L, W_R^*)) + p_1 \mathcal{A}^{(p)}(\Phi(s_1, W_L, W_R^*)) + p_{nG} \mathcal{A}^{(p)}(\Phi(s_{nG}, W_L, W_R^*)). \tag{62}$$

If we introduce the variable $\zeta = \dfrac{\sum_{j=2}^{nG-1} p_j \mathcal{A}^{(p)}(\Phi(s_j, W_L, W_R^*))}{\sum_{j=1}^{nG} p_j}$, we obtain:

$$\zeta_{i+1/2} = \frac{(\widehat{\mathcal{A}^{(p)}})_{i+1/2}^{-} - p_1 \mathcal{A}^{(p)}(\Phi(s_1, W_L, W_R^*)) - p_{nG} \mathcal{A}^{(p)}(\Phi(s_{nG}, W_L, W_R^*))}{1 - p_1 - p_{nG}}. \tag{63}$$

Therefore, (62) become:

$$(\widehat{\mathcal{A}^{(p)}})_{i+1/2}^{-} = (1 - p_1 - p_{nG})\zeta_{i+1/2} + p_1 \mathcal{A}^{(p)}\left(\Phi(s_1, W_L, W_R^*)\right) - p_{nG} \mathcal{A}^{(p)}\left(\Phi(s_{nG}, W_L, W_R^*)\right). \tag{64}$$

Using the same technique, we can propose:

$$\widehat{\mathcal{A}}_{i+1/2}^{+} = (1 - p_1 - p_{nG})\zeta_{i+1/2} + p_1 \mathcal{A}^{(p)}\left(\Phi(s_1, W_R, W_L^*)\right) - p_{nG} \mathcal{A}^{(p)}\left(\Phi(s_{nG}, W_R, W_L^*)\right) \tag{65}$$

Remark 4.3. *Three waves HLL solver has been used here, three waves HLLC3 solver and five wave HLLC5 approximate Riemann solvers also can be constructed by using the generalized jump conditions. The HLL solver contains the slowest and fastest waves in our model; the HLLC3 solver which includes the contact wave and the HLLC5 solver which includes all five waves can be used.*

4.4 Numerical approximation of advection system.

To construct a numerical approximation for advection system, we use the following approach:

$$F^{(a)}(W) = \begin{pmatrix} 0, \\ q^2/h \\ 0 \\ q_b \end{pmatrix} = q \begin{pmatrix} 0, \\ q/h \\ 0 \\ q_b/q \end{pmatrix}.$$

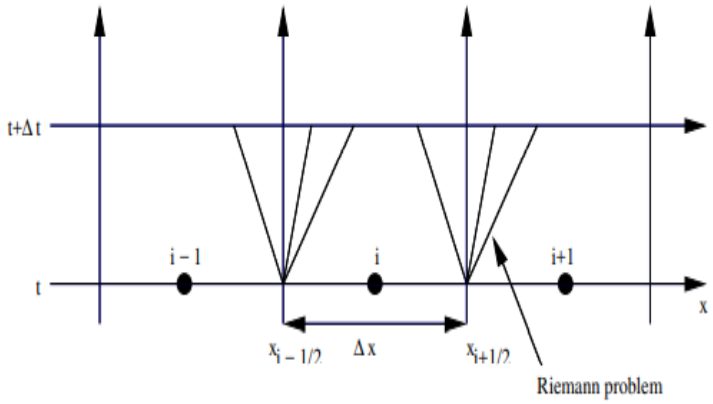

Figure 2: The solving of Riemann problem between neighbouring cells

The flux $\mathcal{F}^{(a)}(W_l, W_R)$ is given by:

$$\mathcal{F}^{(a)}(W_l, W_R) = \max(q^*, 0). \begin{pmatrix} 0, \\ q_L/h_L \\ 0 \\ q_{bL}/q_L \end{pmatrix} + \min(q^*, 0). \begin{pmatrix} 0, \\ \alpha q_R/h_R \\ q_{bR}/q_R \\ 0 \end{pmatrix} \tag{66}$$

where q^* is given by (57).

Remark 4.4. *Finally, for the pressure system, the solution of the Riemann problem W_R^* and W_L^* is evaluated using Eq.(49) at each interface. Then $D^+_{i-1/2}, D^-_{i+1/2}$ are evaluated as in 43 with the matrices evaluated using Gaussian point (58)-(60). The flux advection is given by (66).*

The fluctuation pressure and advection flux now known we can construct the first order semi-discrete scheme without difficulties. An extension of the scheme is obtained by a special algorithms presented bellow.

5 Numerical resolution

This section presents a first-order semi-discrete FVS scheme to solve the proposed model. Next the first order semi-discrete scheme is extended to second order semi-discrete scheme by a modified AENO reconstruction procedure.

5.1 First order FVS scheme

We consider the cell $K_i = \left[x_{i-1/2}, x_{i+1/2}\right]$, we assume at a certain time $t \in (t, t+\tau]$ that the cell averaged of the solution

$$\overline{W}_i(t) = \frac{1}{mes(K_i)} \int_{K_i} W(x,t)dx \quad x \in K_i, \tag{67}$$

is available.

The semi-discrete first order splitting scheme is given by:

$$\frac{d\overline{W}_i(t)}{dt} = \frac{1}{mes(K_i)} \left[\left(D^+_{i+1/2} + D^-_{i+1/2} \right) + \left(\mathcal{F}^{(a)}_{i+1/2} - \mathcal{F}^{(a)}_{i-1/2} \right) \right] + \widehat{S}(\overline{W}_i(t)), \tag{68}$$

where $D^{\pm}_{i+1/2} = D^{\pm}_{i+1/2}(W_L, W_R)$ are the fluctuation due to pressure found at cells boundaries and which are obtained by Riemann problems between cells i, $i+1$ and $i-1$, i (see Eq. (60 with Eqs.(64)-(65), while

$\mathcal{F}^{(a)}_{i+1/2} = \mathcal{F}^{(a)}(W_i, W_{i+1})$ and $\mathcal{F}^{(a)}_{i-1/2} = \mathcal{F}^{(a)}(W_{i-1}, W_i))$ are the numerical advection fluxes obtained by the following technique:

$$\mathcal{F}^{(a)}_{i+1/2} = \max(q^*, 0). \begin{pmatrix} 0, \\ u_i \\ 0 \\ \mu(u_i)^3/(w_i - b_i) \end{pmatrix} + \min(q^*, 0). \begin{pmatrix} 0, \\ u_{i+1} \\ 0 \\ \mu(u_{i+1})^3/(w_{i+1} - b_{i+1}) \end{pmatrix}. \tag{69}$$

They are constant across interfaces between cells during the time step. This technique also can be called advection method. The source term present in Eq.(68) $\widehat{S}(\overline{W}_i(t)) = \dfrac{1}{mes(K_i)} \int_{K_i} \widehat{S}(W(x,t))dx$.

Remark 5.1. *The resulting first-order accurate method is extended to second order accuracy in space via an modified AENO nonlinear reconstruction technique presented here. We recall that following Godunov's theorem [22] the reconstruction must be nonlinear.*

5.2 Second order scheme: Modified AENO reconstruction procedure

Here, we adopt a nonlinear reconstruction procedure to achieve second accuracy in space. This reconstruction technique is obtained by modification of the one proposed by [45]. The technique proposed here is based on AENO technique which an averaged variant of the popular ENO method. The modified AENO reconstruction method is in fact the averaging of two polynomials in the frame of the ENO scheme to choose the reconstruction stencil. Here, a original one-dimensional version of AENO nonlinear reconstruction is presented to improve numerical solutions (which allows to achieve the second order accuracy in space of the scheme). We start by let a piecewise operator of the form:

$$P_i(x) = \overline{W}_i + \Delta_i(x - x_i); \quad x \in K_i \tag{70}$$

where $\Delta_i = (\nabla W)_i$ are the slopes that approximate $(\nabla W(x_i, t^n)$ the slope nonlinearly obtained by convex combination of $\Delta_{i+1/2}$ and $\Delta_{i-1/2}$.

Δ_i can then express as weighted average.

$$(\nabla W)_i = \beta\Delta_{i+1/2} + (1-\beta)\Delta_{i-1/2}, \quad 0 < \beta \leq 1 \tag{71}$$

we have taken:

$$\beta(r) = \frac{r}{\sqrt{\epsilon^2 + r^2}} \text{ with } r = \frac{\Delta_{i-1/2}}{\Delta_{i+1/2} + TOL}. \tag{72}$$

The gradient in Eq.(71) is defined by:

$$\Delta_{i+1/2} = \frac{\overline{W}_{i+1} - \overline{W}_i}{\Delta x}, \text{ and } \Delta_{i-1/2} = \frac{\overline{W}_i - \overline{W}_{i-1}}{\Delta x}. \tag{73}$$

ϵ is a positive parameter, and TOL is a small positive tolerance to avoid division by zero. The result of reconstruction procedure is a non-oscillatory linear polynomial P_i defined at time t^n inside each cell K_i. We remark AENO is a nonlinear polynomial reconstruction procedure that is akin to both existing ENO and WENO procedures. In fact AENO is simple averaged ENO-type method, in which the classical ENO polynomial is averaged with its closest neighbor.

Remark 5.2. *Although this reconstruction eliminates the oscillations and provides a nonlinear stability to the scheme, it does not ensure the positivity of the reconstruction values $h^+_{i+1/2}$ and $h^-_{i+1/2}$ even when average $\overline{h}_i$ is positive for all i. In this work we propose a positivity preserving reconstruction.*

5.3 Well-balanced discretization of source terms

In our method, the discretization of the source terms in (68) is carried out such that the numerical scheme is well balanced with discretization of the flux gradients using the concept of well-balanced. The well-balanced condition is given by:

$$E - D = 0, \quad hC = K_0, \quad h + b = w_0, \quad u = 0, \quad \rho = C_0. \tag{74}$$

We make the treatment of source terms such that the condition (74) is preserved at discrete level. Assuming a stationary flow at rest $u = 0$, a stationary solution ($\mathbf{W}_i^{n+1} = \mathbf{W}_i^n$) is obtained when the gradient and source terms should be equal to zero. Hence if the source terms in the corrected stage of (68) are discretized as:

$$S_{e,i} = \begin{pmatrix} \dfrac{E-D}{1-p} \\ -\dfrac{(E-D)u_i}{(1-p)} \\ E-D \\ -\dfrac{E-D}{1-p} \end{pmatrix}, \quad S_{F,i} = \begin{pmatrix} 0 \\ -g\dfrac{\left(h^-_{i+1/2} + h^+_{i-1/2}\right)}{2} S_{f,i} \\ 0 \\ 0 \end{pmatrix}$$

Then our scheme with this source terms discretization is well-balanced. It is very important for a scheme to satisfy this property.

6 C-property and preserving-positivity of water height.

It is important for an numerical methods to satisfy the so-called C-property and to maintain the positivity of water height. A numerical scheme that does not satisfy the C-property can leads to loss of robustness.

6.1 Verification of C-property

The so-called C-property (or equilibria property) is introduced by Bermudez and Vazquez [7]. It an fundamental property that should verify a numerical scheme. To prove the C-property of our splitting AENO scheme, we start by considering a quiescent flow ($q = 0m^2/s$) over any submerged bed profile the water level $w_i = b_i + h_i$ is constant in the time under these conditions. Generally we have $\dfrac{d\overline{W}}{dt} = 0 \Rightarrow W(t + \Delta t) = W(t) \quad t \in (0, T), \quad \Delta t > 0$

and consequently from (68), we prove that

$$\left(D^+_{i+1/2} + D^-_{i+1/2}\right) + \left(\mathcal{F}^{(a)}_{i+1/2} - \mathcal{F}^{(a)}_{i-1/2}\right) = 0. \tag{75}$$

First we consider the advection flux given by (66). Because $q = 0$ and $huC = 0$, we have $q_L = q_R = 0$ ($h_L u_L = h_R u_R = 0$) and $h_L u_L C_L = h_R u_R C_R = 0$. Consequently we obtain from equation (57):

$$u^* = \frac{Q_{RL}}{h_L(\lambda_L) - h_R(\lambda_R)} \tag{76}$$

where $Q_{RL} = \left[\left|\dfrac{1}{2}gh^2 + \dfrac{g\delta\rho}{2\rho}h^2C\right|\right] + \mathcal{B}^{(2)}(W_L, W_R) + \mathcal{C}^{(2)}(W_L, W_R)$. We can rewrite u^* as follows:

$$q^* = \frac{1}{(\lambda_L) - (\lambda_R)}\left(\left[\left|\frac{1}{2}gh^2\right|\right] + \left[\left|g\frac{\delta\rho}{2\rho}h^2C\right|\right] + \mathcal{B}^{(2)}(W_L, W_R) + \mathcal{C}^{(2)}(W_L, W_R)\right) \tag{77}$$

Using hydrostatic reconstruction method, we have:

$$\widehat{B}_i = \{gh\partial_x b\} = \frac{1}{\Delta x}\int_{K_i} g\bar{h}\frac{\partial b}{\partial x}dx = \frac{1}{\Delta x}\int_{K_i} g\frac{\partial}{\partial x}(\frac{g\bar{h}^2}{2})dx = -\frac{1}{\Delta x}\left[\frac{g\bar{h}^2_{i+1/2_-}}{2} - \frac{g\bar{h}^2_{i-1/2_+}}{2}\right] \tag{78}$$

where

$$\bar{h}^-_{i+1/2} = \min(w_L - b^-_{i+1/2}, h_L), \quad \bar{h}^+_{i+1/2} = \min(w_R - b^+_{i-1/2}, h_R), \tag{79}$$

with

$$\bar{b}^+_{i-1/2} = \min(\max(b_L, b_R), w_R) \quad \bar{b}^+_{i+1/2} = \min(\max(b_R, b_L), w_L) \tag{80}$$

Thus setting

$$h_L = \max(0, \bar{h}^+_{i-1/2}), \quad h_R = \max(0, \bar{h}^-_{i+1/2}), \tag{81}$$

we obtain the following relation:

$$\widehat{B}_i = \frac{1}{\Delta x}\left[\frac{1}{2}gh_L^2 - \frac{1}{2}gh_R^2\right]. \tag{82}$$

Likewise, we have

$$\begin{aligned} \widehat{C}_i &= \left\{\frac{g\delta\rho}{2\bar{\rho}}\left(h\partial_x(hC) - hC\partial_x h\right)\right\} \\ &= \frac{g\delta\rho}{2\bar{\rho}}\frac{1}{\Delta x}\int_{K_i}\left(h\partial_x(hC) - hC\partial_x h\right)dx \\ &= \frac{g\delta\rho}{2\bar{\rho}}\frac{1}{\Delta x}\left(\int_{K_i}\{\{h\}\}\partial_x(hC)dx - \int_{K_i}\{\{hC\}\}\partial_x h dx\right) \end{aligned} \tag{83}$$

Therefore, we obtain:

$$\widehat{C}_i = \frac{g\delta\rho}{2\rho}\frac{1}{\Delta x}\left[h_R h_L (C_R - C_L)\right] \tag{84}$$

This is different from the result that one could obtain with the formulation $gh^2\dfrac{\partial C}{\partial x}$. In fact $(\bar{h})^2 \neq \bar{h^2} \neq h_L h_R$.

$$\overline{q}^{\pm}_{i+1/2} = \overline{h}^+_{i+1/2}\overline{u}^+_{i+1/2}, \quad \overline{(\bar{h}\overline{C})}^{\pm}_{i+1/2} = \overline{h}^{\pm}_{i+1/2}\overline{C}^{\pm}_{i+1/2} \tag{85}$$

Thus $q^* = 0$ into advection scheme (66), we have well $\mathcal{F}^{(a)}_{i+1/2} = 0$. Analogous conclusions can be draw for $\mathcal{F}^{(a)}_{i-1/2}$.

We now have demonstrated that $D^+_{i+1/2} + D^-_{i+1/2} = 0$. Next we focus on the fluctuations $D^+_{i+1/2}$.

$D^-_{i+1/2} = (\widehat{\mathcal{A}^{(p)}})^+_{i+1/2}[W_R - W^*_L]$ where $(\widehat{\mathcal{A}^{(p)}})^+_{i+1/2} = \int_0^1 \mathcal{A}^{(p)}(\Phi(s, W_L, W^*_R))ds$.

Φ is given by Eq.(59) and $\mathcal{A}^{(p)}$ is the Jacobien of pressure sub-system given by Eq.(86). The fluctuation writes

$$D^-_{i+1/2} = \begin{bmatrix} 0 & 1 & 0 & 0 \\ g\bar{h} - \dfrac{\delta\rho}{2\rho}g\overline{hC} & 0 & \dfrac{\delta\rho}{2\rho}g\bar{h} & g\bar{h} \\ -F_{cor}uC & F_{cor}C & F_{cor}u & 0 \\ 0 & 0 & 0 & 0 \end{bmatrix} \begin{pmatrix} h_R - h^*_L \\ 0 \\ h_R C_R - h^*_L C^*_L \\ b_R - b_L \end{pmatrix} \tag{86}$$

with $\overline{hC} = \int_0^1((hC)_L + s((hC)^*_R - (hC)_L)ds$ and $\bar{h} = \int_0^1(h_L + s(h^*_R - h_L)ds$. That is:

$$D^-_{i+1/2} = \begin{pmatrix} 0 \\ \left(g\bar{h} - \dfrac{\delta\rho}{2\rho}g\overline{hC}\right)(h_R - h_L) + \dfrac{g\delta\rho}{2\rho}\bar{h}\left(h_R C_R - h^*_L C^*_L\right) + gh(b_R - b_L) \\ 0 \\ 0 \end{pmatrix} \tag{87}$$

We note that $u^* = 0$, and w is constant $w_R = w_L = w$. according to equation (74), we have $h_L^* = h_L$, $h_R^* = h_R$. Moreover we have $Q_{LR} = 0$ which implies that $h_R = h_L$. Therefore, the second components of $D_{i+1/2}^+$ becomes zero. We proceed in the same for the calculation of $D_{i+1/2}^+$ and will also get $D_{i-1/2}^+ = 0$. Therefore we have proved that:

$$D_{i-1/2}^- + D_{i-1/2}^+ + \mathcal{F}_{i+1/2}^{(a)} - \mathcal{F}_{i-1/2}^{(a)} = 0 \tag{88}$$

which means that the first order scheme is exactly well-balanced. We prove our tests proposed that the second order scheme proposed is also well-balanced.

6.2 Positivity of water height

The intermediate water height h_R^*, h_L^* defined in Eq.(49) do not ensure preservation positivity of water height. For our problem, we propose to address this issue, by used an technique developed by [1] which consist to modify the water height h_R^*, h_L^* preserving the positivity of these values. This technique is also used by [5]. Really, the positivity of h_R^* and h_L^* depends of sign of $\Delta b = \dfrac{mes(K)\langle S\rangle_K}{\Phi}$.

We can easily see that if $\Delta b \geq 0$, then $h_R^* > 0$ and if $\Delta b < 0$, then $h_L^* > 0$. We have two configuration followings:

1) if $\Delta b \geq 0$,

$$\begin{aligned} \lambda_R \widetilde{h}_R^* &= \lambda_R \max(h_R^*, \epsilon), \\ -(\lambda_R \widetilde{h}_R^* - \lambda_L \widetilde{h}_L^*) &= -(\lambda_R - \lambda_L) h_{HLL}, \\ -(\lambda_R h_R^* - \lambda_L h_L^*) &= -(\lambda_R - \lambda_L) h_{HLL}. \end{aligned} \tag{89}$$

2) if $\Delta b < 0$,

$$\begin{aligned} \lambda_L \widetilde{h}_L^* &= \lambda_L \max(h_L^*, \epsilon), \\ \lambda_R \widetilde{h}_R^* - \lambda_L \widetilde{h}_L^* &= (\lambda_R - \lambda_L) h_{HLL}, \\ \lambda_R h_R^* - \lambda_L h_L^* &= (\lambda_R - \lambda_L) h_{HLL}. \end{aligned} \tag{90}$$

We can see easily that the modification preserve the positivity of water height when $\epsilon = \min(0, \min(h_L, h_R, h_{HLL})$. The value of $\widetilde{h}_R^*$ could be h_R^* or ϵ. In the first situation $\widetilde{h}_L^* = h_L^*$ which is positive, and in the second situation ones has
$\widetilde{h}_L^* = h_L^* - \dfrac{\lambda_R}{\lambda_L} h_R^* + \dfrac{\lambda_R}{\lambda_L}\epsilon$.
We apply the same manner in the case when $\Delta b < 0$.

Remark 6.1. *The above semi-discrete scheme given by (68) is proven to be second-order in space, well-balanced and preserving-positivity of the water depth. To achieve the second-order in time, we propose to use a new high-order finite volume time discretization method coupled with a special flux-based resolution algorithm.*

7 New Flux time-steps algorithm discretization procedure

High-order finite volume time discretization methods are often used to reach accuracy requirements as well as low dissipation and dispersion errors.
For the ODEs $\dfrac{d\overline{W}_i(t)}{dt} = RHS(t, \overline{W}_i(t))$ the general s-stage RK method written following:

$$\overline{W}_i^{n+1} = \overline{W}_i^n + f \sum_{k=1}^{s} l_k v_k \tag{91}$$

with

$$v_k = RHS\left(t^n + fm_k, \overline{W}_i^n + f\sum_{k=1}^{s} n_{k,j}v_j\right), \tag{92}$$

and where $m_k = \sum_{k=1}^{s} n_{k,j}, k = 1, ..., s..$ $l_k, m_k, n_{j,k}$ are function on the technique used. Some RK-type methods were developed to solve hyperbolic systems (see[23],[42]), Shallow water equations (see[15]) more general initial value problems with accuracy. The classical Runge-Kutta procedure is not appropriate to solve the sediment transport problem. Because during the simulation, the topography can be partially flooded. In such a situation, the time step must be modified. Bollerman et al [**?**] have proposed the concept of draining time. This concept is valid only in presence of fixed topography. In sediment transport problems, the topography depends on time. And during its evolution, the water depth can be negative ($\overline{Z}_{bj}^n > \overline{h}_j^n$) and generate some numerical instabilities. In this work, an algorithm that estimates the time steps for each stage of the time discretization method is proposed. This procedure maintain the fully discrete scheme stable and guarantees the positivity of water depth in each stage of the time discretization method. This section presents a original way to treat the friction source term, and capital to maintain the discrete balance between the fluxes, and all the source terms.The classical CFL condition cannot guarantee the positivity of the water depth in the presence of a dry zone. In this section, a flux time-steps algorithm that integrates the fact that during a simulation of the cell in the presence of a dry zone is proposed and implemented for our problem. Let us discretize the interval into sub-intervals $[t^n, t^{n+1}]$ with step size and we use the notation $\overline{W}_i^n$ to denote the value of the$\overline{W}_i$ at time t^n. Eq.(68) is a time-independent ordinary differential equation (ODEs). The (ODEs) with the presence of bottom friction, should be solved rigorously by astable, efficient. Moreover, the technique used is able to exactly preserve the steady states and positivity of water depth. We use here a variant of SSP-RK called semi-implicit Runge-Kutta method (SI-RK) based ona modification of the explicit SSP-RK method. The method is developed by[15] and used for the first time for a Shallow water problem. We will implement this method with an original algorithm for our fully coupled sediment transport model to the positivity of the water depth. We start by rewrite the Eq.(68) as follows:

$$\begin{aligned}
\frac{d\overline{w}_i}{dt} &= \mathcal{L}^{(1)}[\overline{W}]_i \\
\frac{d\overline{q}_i}{dt} &= \mathcal{L}^{(2)}[\overline{W}]_i + \mathcal{Z}[\overline{W}]_i q_i \\
\frac{d\overline{(hC)}_i}{dt} &= \mathcal{L}^{(3)}[\overline{W}]_i \\
\frac{d\overline{b}_i}{dt} &= \mathcal{L}^{(4)}[\overline{W}]_i
\end{aligned} \tag{93}$$

where

$$\begin{aligned}
\mathcal{L}^{(1)} &= \mathcal{F}^{(1)} + S_F^{(1)} + S_e^{(1)}, \\
\mathcal{L}^{(2)} &= \mathcal{F}^{(2)} + S_F^{(2)} + S_e^{(2)}, \\
\mathcal{L}^{(3)} &= \mathcal{F}^{(3)} + S_F^{(3)} + S_e^{(3)}, \\
\mathcal{L}^{(4)} &= \mathcal{F}^{(4)} + S_F^{(4)} + S_e^{(4)}.
\end{aligned} \tag{94}$$

with $\mathcal{F} = D_{i+1/2}^{-} + D_{i+1/2}^{+} + \mathcal{F}_{i+1/2}^{(a)} - \mathcal{F}_{i-1/2}^{(a)}$, and where $\mathcal{Z}[\overline{W}]_i = -\dfrac{(E-D)}{\overline{h}_i(1-p)} + C_f|q_i|$.

Using an approach of [15], resulting fully-discrete FVS scheme is described in three steps follows:

Steps 1

$$\begin{aligned}
\overline{w}_i^{(1)} &= \overline{w}_i^n + \delta t \mathcal{L}^{(1)}[\overline{W}]_i \\
\overline{q}_i^{(1)} &= \frac{(\overline{q}_i^n + \delta t \mathcal{L}^{(2)}[\overline{W}]_i)}{1 - \delta t \mathcal{Z}[\overline{W}]_i} \\
\overline{hC}_i^{(1)} &= \overline{hC}_i^n + \delta t \mathcal{L}^{(hC)}[\overline{W}]_i \\
\overline{b}_i^{(1)} &= \overline{b}_i^n + \delta t \mathcal{L}^{(4)}[\overline{W}]_i
\end{aligned}$$

Steps 2

$$\begin{aligned}
\overline{w}_i^{(2)} &= 0.75\overline{w}_i^n + 0.25\left(\overline{w}_i^{(1)} + \delta t \mathcal{L}^{(1)}[\overline{W}^{(1)}]_i\right) \\
\overline{q}_i^{(2)} &= 0.75\overline{q}_i^n + 0.25\frac{(\overline{q}_i^{(1)} + \delta t \mathcal{L}^{(2)}[\overline{W}^{(1)}]_i)}{1 - \delta t \mathcal{Z}[\overline{W}^{(1)}]_i} \\
\overline{hC}_i^{(2)} &= 0.75\overline{hC}_i^n + 0.25\left(\overline{hC}_i^{(1)} + \delta t \mathcal{L}^{(3)}[\overline{W}^{(1)}]_i\right) \\
\overline{b}_i^{(2)} &= 0.75\overline{h}_i^n + 0.25\left(\overline{b}_i^{(1)} + \delta t \mathcal{L}^{(4)}[\overline{W}^{(1)}]_i\right)
\end{aligned} \tag{95}$$

Steps 3

$$\begin{aligned}
\overline{w}_i^{(3)} &= 2/3\overline{w}_i^n + 2/3(\overline{w}_i^{(2)} + \delta t \mathcal{L}^{(1)}[\overline{W}^{(2)}]_i) \\
\overline{q}_i^{(3)} &= 2/3\overline{q}_j^n + 2/3\frac{(\overline{q}_i^{(2)} + \delta t \mathcal{L}^{(2)}[\overline{W}^{(2)}]_i)}{1 - \delta t \mathcal{Z}[\overline{W}^{(2)}]_i} \\
\overline{hC}_i^{(3)} &= 2/3\overline{hC}_i + 2/3(\overline{hC}_i^{(2)} + \delta t \mathcal{L}^{(3)}[\overline{W}^{(2)}]_i) \\
\overline{b}_i^{(3)} &= 2/3\overline{b}_i^n + 2/3(\overline{Z}_{b,i}^{(2)} + \delta t \mathcal{L}^{(4)}[\overline{W}^{(2)}]_i)
\end{aligned}$$

Fully discrete AENO scheme

$$\begin{aligned}
\overline{w}_i^{(n+1)} &= \overline{w}_i^{(3)} \\
\overline{q}_i^{(n+1)} &= \frac{\overline{q}_i^{(3)} - (\delta t)^2 \mathcal{L}^{hu}[\overline{W}^{(3)}]_i}{1 + (\delta t \mathcal{Z}[\overline{W}^{(3)}]_i)^2} \\
\overline{hC}_i^{(n+1)} &= \overline{hC}_i^{(3)} \\
\overline{b}_i^{(n+1)} &= \overline{b}_i^{(3)}
\end{aligned}$$

where $\overline{W}^{(1)} = (w^{(1)}, q^{(1)}, (hC)^{(1)}, b^{(1)})^T$, $\overline{W}^{(2)} = (w^{(2)}, q^{(2)}, (hC)^{(2)}, b^{(2)})^T$, $\overline{W}^{(3)} = (w^{(3)}, q^{(3)}, (hC)^{(3)}, b^{(3)})^T$.

The numerical stability is imposed by the Courant-Friedrichs-Lewy condition and the time step is evaluated as:

$$\Delta t \leq CFL \frac{mes(K_i)}{\max_{1 \leq i \leq 4}(\lambda_i)} \tag{96}$$

where λ_i are the eigenvalues of Jacobian matrix $\mathcal{A}(W)$ defined in Eq.(22).

The classical time step restriction given by Eq.(96) cannot guarantee the positivity of $\overline{h}_i^{(1)} = \overline{w}_i^{(1)} - \overline{b}_i^{(1)}$ for all i provided $\overline{h}_i^n \geq 0, \quad \forall i$.

We can express $\overline{h}_i^{(2)}$ and $\overline{h}_i^{(3)}$ and $\overline{h}_i^{n+1}$ as combination of positive water height h_R^*, h_L^*, h_R, h_L with positive coefficients.

To guarantee the positivity of the water depth at each time step, we propose the following algorithm:

Lemme 7.1. ***The flux time-step algorithm***
(i) $\overline{h}_i^{(1)} \geq 0$ *for all* i *provided that* $\Delta t \leq \min(\Delta t^*, \Delta t^I)$ *with*

$$\Delta t^I := \frac{\Delta x \overline{h}_i^n}{\max(0, \mathcal{F}^{(1)})} \tag{97}$$

(ii) $\overline{h}_i^{(2)} \geq 0$ *for all* i *provided that* $\Delta t \leq \min(\Delta t^*, \Delta t^{II})$ *with*

$$\Delta t^{II} := \frac{\Delta x \min(3\overline{h}_i^n, \overline{h}_i^{(1)})}{\max(0, \mathcal{F}^{(1)}[W^{(1)}])} \tag{98}$$

(iii) $\overline{h}_i^{(3)} \geq 0$ *for all* i *provided that* $\Delta t \leq \min(\Delta t^*, \Delta t^{III})$ *with*

$$\Delta t^{III} := \frac{\Delta x \min(3\overline{h}_i^n, \overline{h}_i^{(2)})}{\max(0, \mathcal{F}^{(1)}[W^{(2)}])} \tag{99}$$

where $\Delta t^* := CFL \dfrac{mes(K_i)}{\max_{1\leq i\leq 4}(\lambda_i)}$

8 Numerical results

All the tests presented here are in dimension one. i.e. $K_i =]x_{i-1/2}, x_{i+1/2}[$. The scheme can however easily be extended in dimension two on cartesian mesh and on unstructured mesh.

In all of the examples in the follows text the gravitation constant $g = 9.81$, the porosity is $p = 0.3$ the AENO reconstruction parameters is given by $TOL = 0.0001$ and $\epsilon = 1$. In these tests the numerical results of our scheme are compared to a reference solution (the exact solution or an approximation of exact solution obtained by refine mesh). The error between the numerical solutions and the reference solution is computed and the convergence rate is deduced. The error is evaluated in $L^p - norm$ at the time $t = T$ where T is the final time.

8.1 Steady states lake at rest.

We begin by illustrating the well balanced property of the designed scheme as also done in [4]. We show that our scheme is able to exactly preserves the steady states solutions. That is, the equilibria (74) are preserved thus satisfy the well-balanced property. Here, the domain of simulation is $\Omega = [0,\ \ 1000]$ and the initial conditions are defined as

$$\begin{cases} b(x,0) = \begin{cases} \sin^2(\dfrac{(x-300)\pi}{200}) & \text{if } 300 \leq x \leq 500, \\ 0 \end{cases} \\ h(x,0) = 10 - b(x,0), \quad u(x,0) = 0, \quad C(x,0) = 0. \end{cases}, \tag{100}$$

The result is computed by using the splitting scheme and presented in Fig. (3).

The result using the condition above are presented in Fig. 3. We easily see that the steady states at rest are respected for a long time simulation moreover, The well-balanced property of the designed scheme is respected. The test prove the ability of the designed scheme to exactly preserve the steady states solution.

It is expected in Fig. (3) that the water free-surface remains constant and the water velocity should be zero at all times.

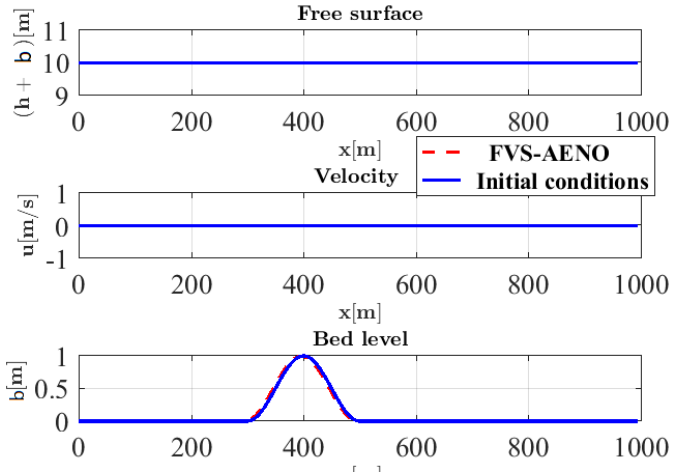

Figure 3: The Steady state at rest over bum. The number of cells is 200, Ag=0.005, t=1000s.

8.2 Accuracy test with Analytical solutions.

We use here our FVS AENO method for solving the Saint-Venant-Exner model given by Eq.(1) an second equation of Eq.(5a) without sediment exchange ($E - D = 0$). Here, in order to test the convergence of our method we solve the system formed by the two (1) ignoring the terms in the right-hand sides except the bottom slope. The bed evolution in equation (5a) is replaced by the Exner's equation with Grass formula ($q_b = Agu^3$). The system obtained is similar of that solved in [45] by a splitting scheme. The system is:

$$\begin{cases} \dfrac{\partial h}{\partial t} + \dfrac{\partial hu}{\partial x} = 0, \\ \dfrac{\partial hu}{\partial t} + \dfrac{\partial}{\partial x}(huu + \dfrac{1}{2}gh^2) = -gh\dfrac{\partial b}{\partial x}, \\ \dfrac{\partial b}{\partial t} + \dfrac{1}{(1-p)}\dfrac{\partial q_b}{\partial x} = 0. \end{cases} \tag{101}$$

The two conservative subsystems obtained by a splitting technique of flux in two others fluxes $F^{(p)}$ and $F^{(a)}$ named pressure and advection fluxes given by:

$$F(W) = \begin{pmatrix} q \\ \dfrac{q^2}{h} + \dfrac{1}{2}gh^2 \\ \dfrac{1}{(1-\lambda)}q_b \end{pmatrix} = F^{(p)} + F^{(a)} \text{ where } F^{(p)} = \begin{pmatrix} hu \\ \dfrac{1}{2}gh^2 \\ 0 \end{pmatrix}, \quad F^{(a)} = \begin{pmatrix} 0 \\ hu^2 \\ q_b \end{pmatrix} \tag{102}$$

The system is hyperbolic and admits smooth solutions. We compare the FVS results with those proposed by Berton et al [5] using analytical method. A great interests of result proposed by [5], is the derivation of numerical benchmarks to valid the numerical scheme. This test is also made by [27],[14]. The analytical solution is given by[5]:

$$\begin{cases} q_{anal}(x) = 1 \\ u_{anal}(x) = \left[\dfrac{\alpha x + \beta}{Ag}\right]^{1/3} \\ h_{anal}(x) = \dfrac{q_{anal}}{u_{ini}} \\ b_{anal}(x) = 1 - \dfrac{u_{anal} + 2gq_{anal}(x)^2}{2gu_{anal}} \end{cases} \tag{103}$$

where the coefficients are given by $\alpha = \beta = Ag = 0.005$. The initial condition are [5]:

$$q = q_0, \quad h(x,0) = q_0(\frac{\alpha x + \beta}{Ag})^{-1/3} \quad b(x,0) = C - \frac{\frac{\alpha x + \beta}{Ag} + 2gq_0}{2g(\frac{\alpha x + \beta}{Ag})^{1/3}} \tag{104}$$

while boundary conditions on the domain $0 \leq x \leq L, \quad L = 10m$ are given by:

$$q(0,t) = q_0 \quad h(L,t) = q_0(\frac{\alpha L + \beta}{Ag})^{-1/3} \quad b(0,t) = C - \alpha t - \frac{\beta/Ag - 2gq_0}{2g(\beta/Ag)^{1/3}} \tag{105}$$

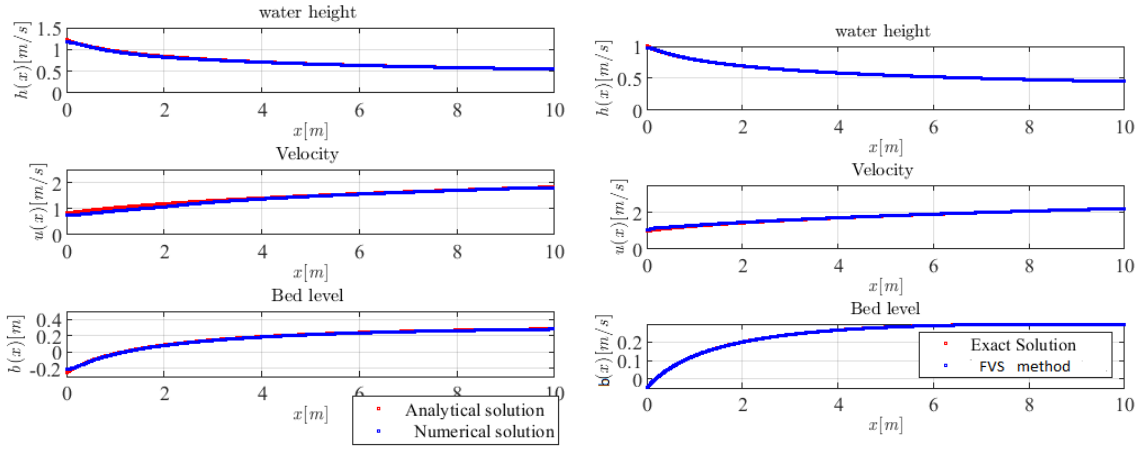

Figure 4: Exact solution. Comparison between exact solution and numerical solution. left N=200, right N=300

One compare the numerical and analytical solutions. The results presented in Fig. (4), demonstrates that the proposed scheme describes the bed level and water height evolution with good accuracy. We can see that the analytical solution is well approximated by FVS method.

	h		u		b	
N	L^1	$\mathcal{O}(L^1)$	L^1	$\mathcal{O}(L^1)$	L^1	$\mathcal{O}(L^1)$
50	7.38E-2	/	2.08E-1	/	3.5E-2	/
100	3.67E-2	1.007	1.19E-1	0.805	3.28E-2	0.977
200	1.79E-2	1.04	6.36E-2	0.903	1.66E-2	0.982
400	8.78E-3	1.027	3.29E-2	0.95	8.32E-3	0.996
800	4.33E-3	1.019	1.67E-2	0.7507	4.17E-3	0.99
1600	2.15E-3	1.01	8.44E-3	0.984	2.09E-3	0.996

Table 1: Error between exact solution and numerical solution in first order accuracy using $CFL = 0.5$

	variable h		variable u		variable b	
N	L^1	$\mathcal{O}(L^1)$	L^1	$\mathcal{O}(L^1)$	L^1	$\mathcal{O}(L^1)$
50	1.16E-2	/	1.14E-1	/	6.54E-3.	/
100	3.59E-3	1.69	5.89E-2	1.95	2.29E-3	1.28
200	1.09E-3	1.81	3.01E-2	1.968	1.13E-3	1.25
400	3.29E-4	1.72	1.53E-2	1.99	5.02E-4	1.17
800	9.49E-5	1.79	7.85E-3	1.966	2.32E-4	1.11
1600	2.6E-5	1.84	4.08E-3	1.944	1.11E-4	1.06 /
3200	6.87E-6	1.93	2.02E-3	1.89	5.43E-5	1.03

Table 2: Estimate error between exact solution and numerical solution of second order FVS scheme using our AENO-based reconstruction. TOL=0.0001, $\epsilon = 1$, CFL $= 0.5$.

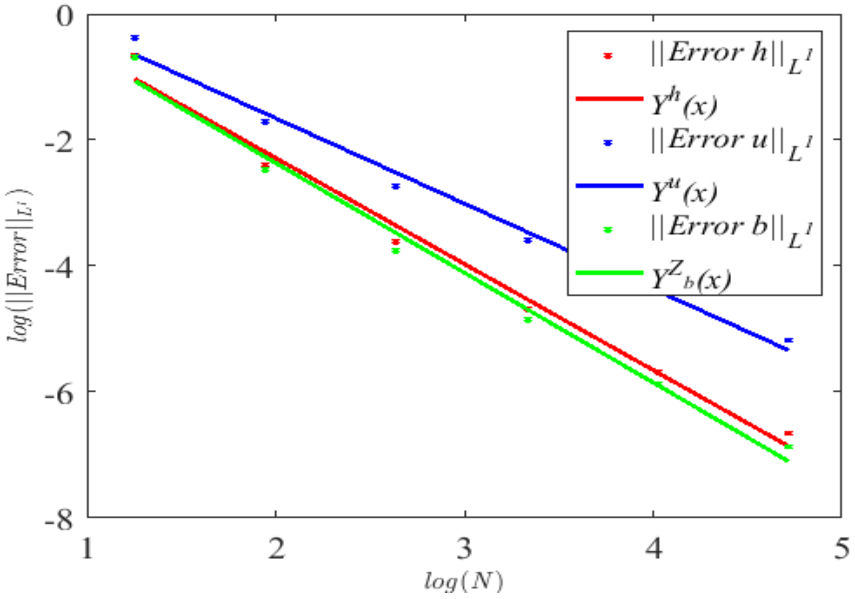

Figure 5: The convergence rate of discrete $L^1 - norm$ error of h and u in various step points Δx . The functions $Y^h(X)$,$Y^q(X)$ and $Y^b(X)$ are obtained from data fitting of $L^p - norm$ error of h , q and b respectively using the nonlinear least-squares method.

(Table1) and (Table2) show the discrete $L^p - norm$,where $p = 1$ of the error for h, q and b in first order and second order respectively at the final time step $t = 7$. We can see clearly that the splitting scheme proposed in this work have a good convergence rate $\mathcal{O}(L^1)$, respectively $\mathcal{O}(L^\infty)$ in various grid number where it tends to 1 since computed in first order.

The good convergence rate of discrete $L^1 - norm$ in h,u and b are shown nicely increasing along with the increasing number of points. The numerical tests show also that our nonlinear slope limiter is very interesting and is able to eliminate of oscillations near the discontinuities.

In Fig. (??) we show how the solution obtained by our method are in good correlation with the regression line.

The functions $Y^h(X)$,$Y^q(X)$ and $Y^b(X)$ are obtained from data fitting of $L^p - norm$ error of h , q and b respectively using the nonlinear least-squares method following the methodology presented below.

8.3 Shallow water system over non erodible bed: comparison with analytical solution.

In this test shallow equation over non erodible is solved using our scheme. So only the hydrodynamical system is used. The test is performed by a dam-break. The fluid velocity $u(0,x) = 0$ and friction term is not introduced; the final time is $T = 30s$. The domains of simulation are $\Omega = [0, 2000]$ for one-dimensional case and $\Omega = [0, 2000] \times [0, 10]$. The dam is located at the middle of Ω. The dam separates two initial water depth exhibits wet zone are $h(0,x) = 40m$ at the left side and $h(0,x) = 2m$ at for the right side of the domain. Numerical results are compared with the exact solutions. The both exact solution and FVS scheme are computed and plotted in Fig. (8). In all cases they are in good agreement and converge to the exact solution.

The equations are similar with Eq.(101) without bed evolution equation. The splitting fluxes are given by:

$$F(W) = \begin{pmatrix} q \\ \frac{q^2}{h} + \frac{1}{2}gh^2 \\ 0 \end{pmatrix} = F^{(p)} + F^{(a)} \quad \text{where} \quad F^{(p)} = \begin{pmatrix} hu \\ \frac{1}{2}gh^2 \\ 0 \end{pmatrix}, \quad F^{(a)} = \begin{pmatrix} 0 \\ hu^2 \\ 0 \end{pmatrix} \tag{106}$$

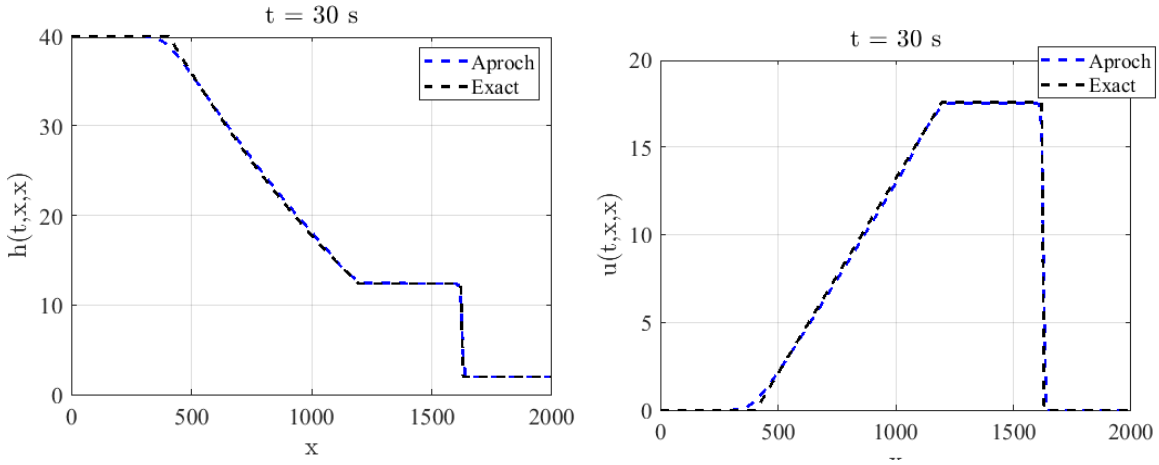

Figure 6: Riemann solution for Saint-Venant system. Comparison between exact solution and numerical solution obtained by FVS method. Left water surface, right velcity

Our numerical proposed here, can be interpreted as a shock-capturing method. We expected that the numerical scheme developed and presented here can treat the discontinuities and capture shocks associated with Dam-break on non erodible beds. The profiles of velocity and water height are well represented and the physical properties of the studied problem are preserved (robustness).

8.4 Bum sediment long time evolution

This test consists to show that the proposed numerical modeling can solve a bum evolution problem. For this case one numerical test on a long time evolution bump for time $t = 1000s$. The initial conditions are:

$$\begin{cases} b(x,0) = 0.1 + 0.1\exp(-(x-5)^2), \quad C(x,0) = 0, \\ h(x,0) = 0.4 - b(x,0), \\ q(x,0) = 0.6. \end{cases} \tag{107}$$

The result is displayed and plotted in Fig. (7).

We observe via the Fig. (7) a good evolution of the topography well in agreement with what we could have observed in nature. No non physical oscillations are observed. The stability and robustness of the scheme is well observed.

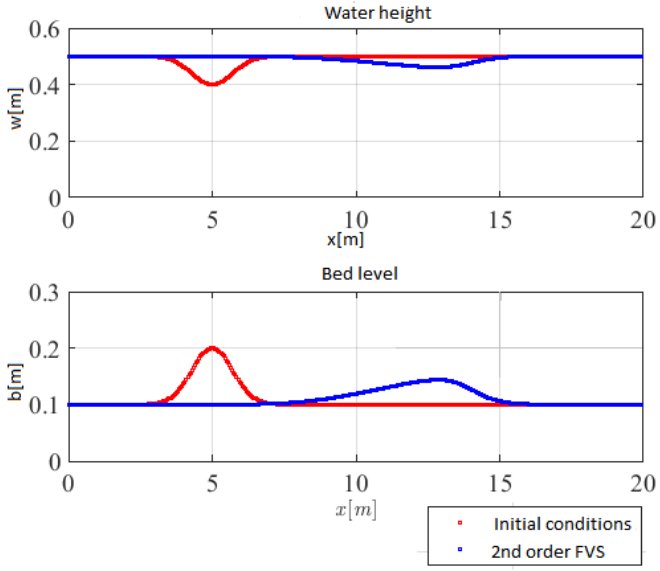

Figure 7: The Steady state at rest over bum in different time simulation. The number of cells is 200, Ag=0.009 without friction source terms. t=1000s.

8.5 Dam break tests over the mobile bed with concentration variation.

A dam-break wave starting out as clear water is likely to rapidly pick up sediment both from the dam body and from the valley floor. Its intensity depends on the available sediment of the region concerned. We present here the numerical result for some test cases of sediment transport in the dam-break problem. The objectives are to assess the performance of the FVS AENO method described above and to prove its capability to solve the dam-break problem over erodible beds. We consider the rectangular channel of length $L = 10m$. The initial conditions for the proposed model are given:

$$h(x,0) = \begin{cases} 10 \text{ if } x \leq 5m \\ 1 \text{ if } x > 5m \end{cases}, \quad u(x,0) = 0m/s, \quad C(x,0) = 0, \quad b(x,0) = 0 \tag{108}$$

The references parameters used here for the simulations are: $\rho_w = 1000Kg/m^3$, $\rho_s = 2650Kg/m^3$, $\varphi = 0.35$, $\nu = 1.2.10^{-6}m^2/s, p = 0.4$, $\rho_0 = 0.03s/m^{1/3}$. A similar test problem can be found in [4],[9]. All the simulation are performed using a mesh grid 400 grid points.

Here, we computed the bed evolution, the free surface and the sediment concentration. The numerical results obtained at four different time and four different grain size are plotted in Fig. (8) and Fig. (9). The accuracy of FVS is studied by setting the diameter of grain size $d = 4mm$. The front of sediment concentration profile is similar to that obtained by refinement of the mesh in the results presented in [4] and not plotted here. It is expected that the solution does not presents numerical diffusion. The AENO based reconstruction eliminate well the numerical diffusion and the nonphysical oscillation near the region of large gradients.

As can be seen from these results (see Fig. (9)),the dam-break over mobile bed can participate in the creation of a highly concentrated wave front, which is limited by the forefront and a sediment transport contact discontinuity, and decreases with time. Bed mobility can influence the water level on the surface and can have considerable implications for flood forecasting. As in previous simulations, a hydraulic jump in the free water surface is initially formed around the dam site,decreases in height as it moves upstream, and finally disappears. It is clear that the moving bed can be scoured significantly and the dimensions of the scour hole

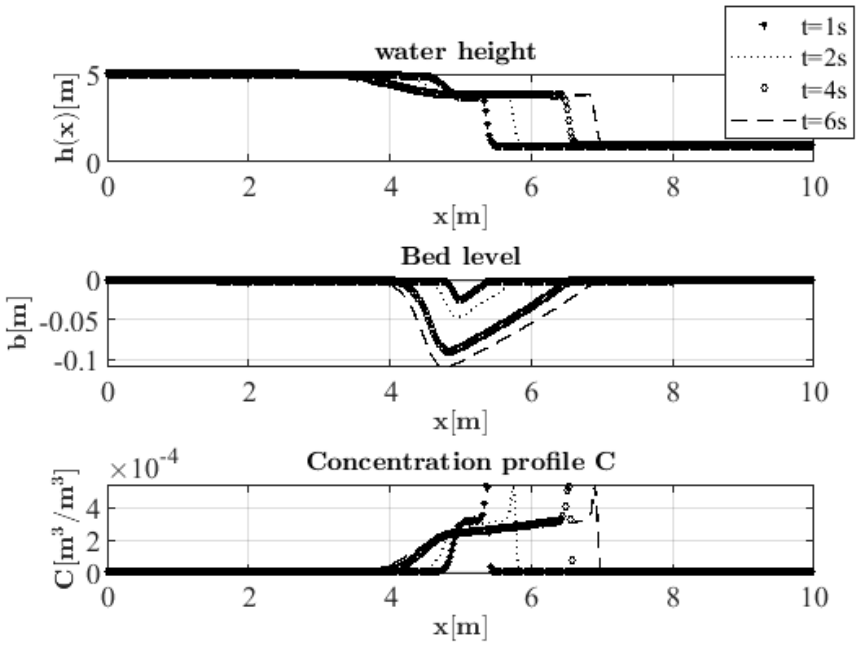

Figure 8: Comparison of bed and water free-surface and sediment concentration at four instant and using same diameter $d = 4mm$

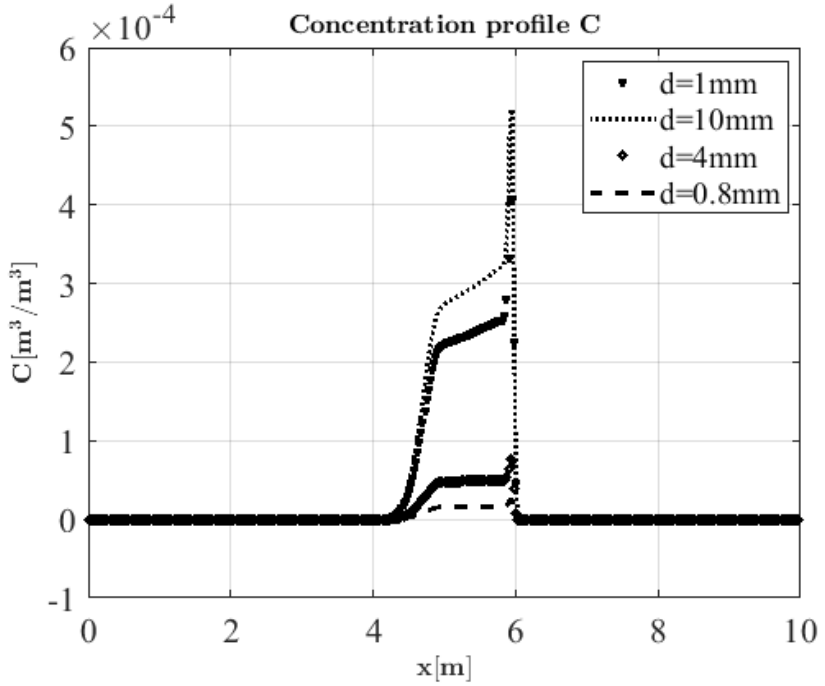

Figure 9: Comparison of different diameter values in sediment concentration at same instant.

are of a similar order of magnitude to those of the water flow itself. Therefore, the deformation rate of the bed is not negligible compared to that of the flow change, hence the need to make use of a numerical coupling as proposed by SI-RK3used in this work. The FVS AENO scheme gives good results for this test problem

since the moving fronts and no spurious oscillations were observed when the water. The FVS AENO scheme performs well for this test problem since it does not scatter the moving fronts and no spurious oscillations were observed when the water flows over the moving bed.
A such explanation is given using hydraulic-based routing models (based on the continuum assumption for both and sediment). In this approach, the property of sediment flow is similar to that of clear water flow. Really the mixture of water-sediment is more dense than clear water. Then Hydraulic-based approach is not adapted to describe the behavior of debris flow due to dam-break. Another reason is the incompatibility of medium (continuous for clear water and noncontinuous continuous for dense mixture of sediment-water). Even if the concentration profile is continuous, the sediment concentration is not really continuous. These result shown that the rheological behavior of a mixture depend on the hydrodynamic characteristic of the flow and the characteristic of sediment(grain size, grain sharp, cohesive property of grain, etc.

$$h(x,0) = \begin{cases} 10 \text{ if } x < 5m \\ 1 \text{ if } x > 5m \end{cases}, \quad u(x,0) = 0m/s, \;\; C(x,0) = 0, \;\; b(x,0) = 0 \tag{109}$$

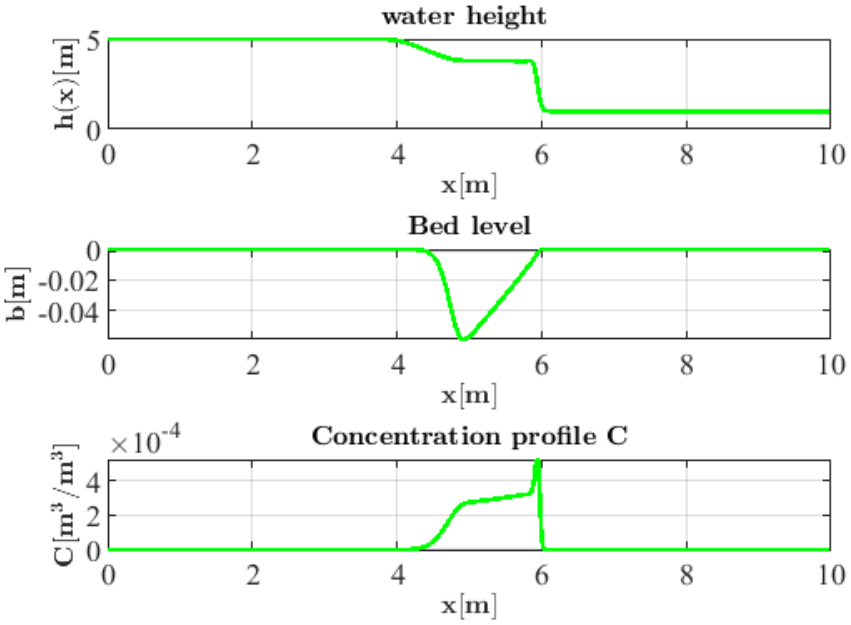

Figure 10: Water depth profile, Bed evolution and concentration profile

Fig. 10 shows that the sediment concentration profile is continuous monotonously and decreases in the vertical direction from the maximum value of $C(x,t)$ at the bed.The velocity profile is also continuous monotonously. The velocity is weak at the initial dam, increases during the propagation of the flow and decrease from the maximum value of $u(x,t)$. The exchange between the water column and the bed is not negligible. The sediment concentration is strongly associated with the fluid velocity which influence also the spatial gradient concentration.

The erosion is more intense at the beginning of the dam than at the end. The water mixes with a large amount of sediment at the first moment of the dam break and this is due to the force of fluid on the moving bed and the porosity bed assumed to be constant in this work.The force of the fluid is proportional to the deep of the bed.This proves the use of a coupled scheme like ours calculating the variation of the water depth $h(x,t)$, the velocity $u(x,t)$, the sediment concentration $C(x,t)$ and the bed evolution $b(x,t)$ at the same time.

8.6 Riemann problem for Saint-Venant-Exner Equations. Comparison between PRICE-C method, DOT-AENO, Splitting-ENO,

Here we reproduced the test made by [45] in second order accuracy. The initial discontinuity is at $x = 0$ and initial data to the left and right are are given in Table.3. The results obtained are compared with other scheme as the PRICE-C method, DOT-AENO, Splitting-ENO and exact solution plotted in [45].

test	$h_L[m]$	$q_L[m^2/s]$	$Z_b[m]$	$h_R[m]$	$q_R[m^2/s]$	$Z_b[m]$
Movable bed	2	0.5	3	2	4.34297	2.84751

ù:b

Table 3: initial condition of Riemann problem

The second order result presented in Fig.11 prove that the proposed FVS method is very sophisticated.

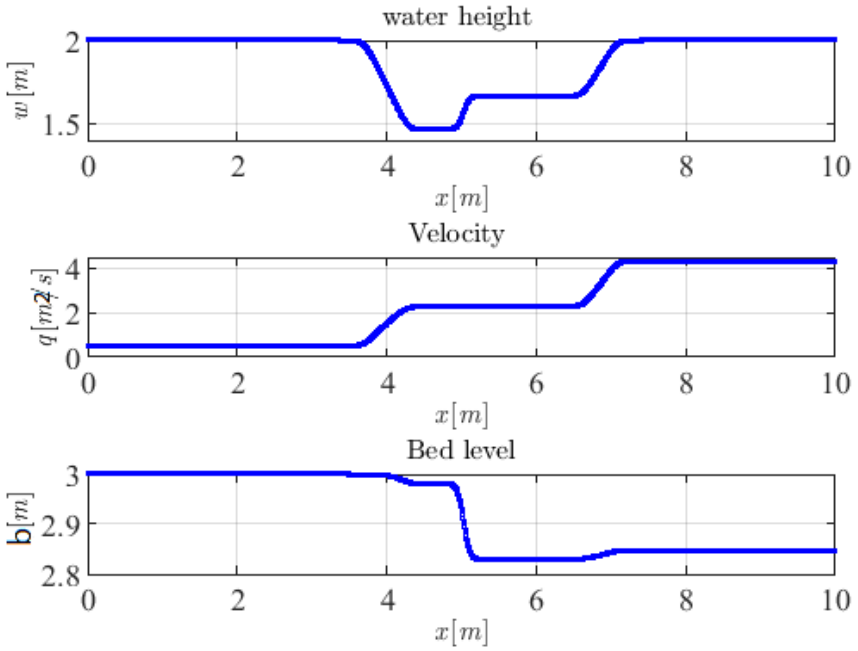

Figure 11: Results for a Riemann problem with movable bed (2nd order of accuracy). Sediment transport is quantified by using Grass sediment transport formula with Ag=0.01 and m=3. Computational parameters are: N=150, domain length L=10m, Tfinal=1s and CFL=0.5. AENO reconstruction is performed using TOL= 0.0001 and $\epsilon = 0.5$.

All the waves are captured by the scheme even on the coarse mesh. The numerical solution and the location of the waves agree well with the exact solution. The numerical results approach the exact solution on the finer mesh as seen in Fig.(11). The scheme gives good results for this test problem, in which the central shock wave moves very slowly. As expected also, the FVS method does not diffuse the central shock wave contrary to other schemes such as the PRICE-C method. The results in the second order are similar form those obtained by DOT-AENO, Splitting-ENO, Splitting-AENO.

8.7 Rate of convergence

Let us $err = |W_{\mathcal{T}}^{ex}(x_K) - W_{\mathcal{T}}^{app}(x_K)|$. where $\mathcal{T} = \bigcup_{K\in\mathcal{P}} K$; and where K is the cell of mesh.
we defined the $L^\infty - norm$ and $L^p - norm$ where $p = 1, 2$ of err of the following manner:

$$\|err\|_{L^\infty} = \|W_{\mathcal{T}}^{ex} - W_{\mathcal{T}}^{app}\|_\infty = \max_{K\in\mathcal{T}} |W_{\mathcal{T}}^{ex}(x_{K_j}) - W_{\mathcal{T}}^{app}(x_K)|; \tag{110}$$

$$\|err\|_{L^p} = \left(\sum_{K_j \in \mathcal{T}} |K_j| |W_{\mathcal{T}}^{ex} - W_{\mathcal{T}}^{app}|^p \right)^{\frac{1}{p}} \tag{111}$$

We defined also the relative error err_{rel} by following formulae:

$$err_rel = \frac{\left(\sum_{K \in \mathcal{T}} |K| \, |W_{\mathcal{T}}^{ex} - W_{\mathcal{T}}^{app}|^p \right)^{\frac{1}{p}}}{\left(\sum_{K \in \mathcal{T}} |K| \, |W_{\mathcal{T}}^{ex}|^p \right)^{\frac{1}{p}}} \tag{112}$$

now we search to define the rate of convergence. We start by setting:
$\|err\|_{L^\infty} = C(\Delta x)^m$, with $m > 0$
$\log \|e_h\|_{L^\infty} = m \log h + \log C$ then we defined the linear regression line Y by $Y = mX + \theta$. We defined the function ψ by:
$\psi(m, \theta) = \sum_{j=1}^{J} \left[(mX_j + \theta) - Y(X_j) \right]^2$ in minimization form is: $\psi(\hat{m}, \hat{\theta}) = \min \psi(m, \theta) \Rightarrow \nabla \psi(\hat{m}, \hat{\theta}) = 0$

the values of m and θ of linear regression line Y are given by resolution the following equations:

$$\begin{cases} \dfrac{\partial \psi}{\partial m}(\hat{m}, \hat{\theta}) = 0 \\ \dfrac{\partial \psi}{\partial \theta}(\hat{m}, \hat{\theta}) = 0 \end{cases} \tag{113}$$

that is

$$\begin{cases} \sum_{j=1}^{J} X_j \left[(mX_j + \theta) - Y_{\mathcal{T}}(X_j) \right] = 0 \\ \sum_{j=1}^{J} \left[(mX_j + \theta) - Y_{\mathcal{T}}(X_j) \right] = 0 \end{cases} \tag{114}$$

$$\begin{cases} (\sum_{j=1}^{J} X_j^2) m + (\sum_{j=1}^{J} X_j) \theta = \sum_{j=1}^{J} X_j Y_j \\ (\sum_{j=1}^{J} X_j) m + I\theta = \sum_{j=1}^{J} Y_j \end{cases} \tag{115}$$

We obtain the rate of convergence m and the value θ:

$$m = \frac{\sum_{j=1}^{J} X_j Y_j - \frac{1}{J} (\sum_{j=1}^{J} X_j)(\sum_{j=1}^{J} Y_j)}{(\sum_{j=1}^{J} X_j^2) - \frac{1}{J} (\sum_{j=1}^{J} X_j)^2}, \quad \theta = -\frac{1}{J} (m \sum_{j=1}^{J} X_j) + \sum_{j=1}^{J} Y_j, \tag{116}$$

where $J = N_i, i = 1, ..., n; n \in \mathbb{N}$ is different number of cells.

9 Conclusion

In this article, a new finite volume splitting AENO method has been proposed to solve a new one-dimensional averaged sediment transport model (also developed here). The model studied here consists to hydro-sediment-morphodynamic coupling equations which describe the morphology evolution and sediment concentration in shallow water flows. The hydro-sediment-morphodynamic coupling is constituted of the Saint-Venant/sediment equations, sediment concentration equation and Exner-type equation.
The designed model presented here is reasonable mathematical tools for modeling some problems in coastal engineering such that dam break flows over erodible sediment beds. We proposed a methodology for their numerical solution based on path-conservative methods with HLL-Riemann solver for space discretization. and Semi Implicit Runge-Kutta technique for time discretization and the fully discrete scheme has been obtained with an second-order accuracy.
The new equations presented here can serve to construct a wave-front in the sediment concentration which is bounded by a contact discontinuity of the sediment transport and decreases in the vertical direction from its maximum value at the bed.
The numerical tests show also that our nonlinear slope limiter is very interesting and is able to eliminate

of oscillations near the discontinuities. We have proved the C-property of our scheme and the positivity of water depth. Finally, we assess the robustness of the scheme considering different test cases. The proposed finite-volume-based method is seen to be stable, accurate and gives a good resolution of hydraulic jump in water free-surface. The scheme described the strong interaction existing between free surface elevation and sediment bed evolution.
The method is consistent with the definition of weak solutions. This consistency makes the FVS-AENO scheme robust and helps to obtain better results than other methods. The numerical results presented here gives the ability of our scheme to achieve very high resolution.Future work is extended to study the numerical solutions of the multi-dimensional case on unstructured mesh. The theoretical convergence of this scheme is a research issue.

Conflict of Interests

The authors declare that there is no conflict of interests regarding the publication of this paper.

Acknowledgment

The authors would like to thank at Laboratory E3M, National Advanced School Polytechnic, University of Douala , P.O.BOX 2107, Douala, Cameroon for their encouraging.

[1] E. Audusse, C. Chalons, and P. Ung., A simple three-wave Approximate Riemann Solver for the Saint-Venant-Exner equations. Communications in Mathematical Sciences, Vol.13(2015), no.5, pp.1317-1332.

[2] J.A. Bailard. An energetics total load sediment transport model for a plane sloping beach. J. Geophys. Res., 86(C11),1981.

[3] Barre de Saint-Venant AJC, Théorie du mouvement non-permanent des eaux, avec application aux crues des rivière et à l'introduction des marées dans leur lit, Comptes Rendus de L'Académie des Sciences 1871; 73:147-154.

[4] Fayssal Benkhaldou, Saida Sari, Mohammed Seaid., A flux-limiter method for dam-break flows over erodible sediment beds. Applied Mathematical Modelling, 36(2012), pp. 4847-4861.

[5] Christophe Berthon, Stéphane Cordier,Olivier Delestre, Minh HoangLe, An analytical solution of the Shallow Water system coupled to the Exner equation, In: Comptes Rendus Mathematique 350.3 (2012), pp. 183-186. doi: 10.1016/j.crma.2012.01.007.

[6] Berthon, C., Boutin, B., Turpault, R. (2015). Shock Profiles for the Shallow-Water Exner Models. Advances in Applied Mathematics and Mechanics, 7(3), 267-294. doi:10.4208/aamm.2013.m331.

[7] Bermudez, A., Vazquez, E., Upwind methods for hyperbolic conservation-laws with source terms. Computers&Fluids 23 (8)1994, pp. 1049-1071.

[8] A. Bhole, B. Nkonga, S. Gavrilyuk, and K. Ivanova. Fluctuation splitting Riemann solver for a non-conservative modeling of shear shallow water flow. Journal of Computational Physics, **392**, (2019), pp. 205-226.

[9] Cao, Z., Pender, G., Wallis, S., and Carling, P. (2004). Computational dam-break hydraulics over 331 erodible sediment bed. J. Hydraul. Eng., 130(7), 689-703.

[10] A. Capart, D. L. Young, Y. Zech Dam-break induced debris flow. Spec, pubs. Int. Ass. Sediment(2001) 31, 149-156.

[11] M.J. Castro, A. Kurganov and T Morales de luna, Path Conservative Central-Upwind for non conservative hyperbolic systems, ESAIN M2AN 53, (2019) pp. 959-985.

[12] M.J.Castro Diaz, E. D,Fernandez Nieto, A .M . Ferreiro. High order extension of Roe schemes for two dimensioal non conservative hyperbolic systems, Journal of Scientific Computing, vol 39(2009), pp. 67-114.

[13] Manuel Castro, José M. Gallardo and Carlos Parés, High Order Finite Volume Schemes Based on Reconstruction of States for Solving Hyperbolic Systems with Nonconservative Products. Applications to Shallow-Water Systems, Mathematics of Computation Vol. 75, No. 255 (Jul., 2006), pp. 1103-1134.

[14] Carraro F., Valiani A. and Caleffi V, Efficient analytical implementation of the DOT Riemann solver for the de Saint Venant-Exner morphodynamic model, Advances in Water Resources, March 2018, pp 189-201.

[15] Chertock .S .Cui, A . Kurganov and W .Tong., Steady state and system preserving semi-implicit Runge-Kutta methods for ODEs with stiff damping term. Inter.J.Num.meth fluids 78,(2015) 355-383.

[16] Mariana. C. A. Clare, James R. Percival, Althanasios Angeloudis, Colin J. Cotter, M. Piggot. Hydro-morphodynamics 2D modelling using a discontinuous Galerkin discretization. Computers&Geosciences 146, 104658, 2021.

[17] Tatyana Dyakonova and Alexander Khoperskov. Bottom friction models for shallow water equations: Manning's roughness coefficient and small-scale bottom heregeneity. Journal of Physics Conference series, 973 (1):012032, doi:10.1088/1742-6596/973/1/012032.

[18] G. Dal Maso, P .G .Lefloch,F . Murat. Defintion and weak stability of nonconservative products. J .Math.Pures Appl.74. 483-548, 1995.

[19] V. Michel-Dansaca, Christophe Berthona, Stéphane Clainb, Françoise Fouchera, A well-balanced scheme for the shallow-water equations with topography. Computers and Mathematics with Applications,72, 2016, pp. 568-593.

[20] Edwige, G. and Raviart, P.A. Hyperbolic Systems of Conservation Laws. Series Mathematics and Applications (1991), Ellipses, Paris.

[21] A .J . Grass, Sediment transport by waves and currents, department of civil engineering, University college, London, 1981.

[22] Godunov, S., A finite difference method for the computation of discontinuous solutions of the equations of fluid dynamics. Sbornik: Mathematics 47 (8-9) 1959, 357-393.

[23] Sigal Gottlieb, Chi-Wang Shu and Eitan Tadmor, Strong stability preserving high order time discretization methods, SIAM Rev., 43(1)2011, 89-112, https://doi.org/10.1137/S003614450036757X.

[24] Greimann, B. P.; Huang, J. C. Two-dimensional total sediment load model equations. J. Hydraul. Eng, 134, 1142-1146.

[25] A.Harten, P Lax and B. van Leer, Upstream differencing and Godunov-type scheme for hyperbolic conservation laws, Upwind and High-Resolution Schemes, 1982, pp. 53-79, DOI: 10.1007/978-3-642-60543-74.

[26] A. Harten, P. D. Lax, and B. van Leer, On upstream differencing and Godunov-type schemes for hyperbolic conservation laws, SIAM Rev., 25 (1983), pp. 35-61.

[27] Harry Putu Gunawan. Numerical simulation of shallow water equations and related models. General Mathematics [math.GM]. Université Paris-Est, 2015. English. NNT: 2015PEST1010. tel-01216642v2.

[28] Holly, F. M. and Rahuel, J. M., New numerical/physical framework for mobile bed modelling, part1: Numerical and physical principles. Journal Hydraul. Res. 1990, 28,401-416.

[29] Huybrechts, N., Villaret, C., Hervouet, J.M., Comparison between 2D and 3D modelling of sediment transport. Application to the dune evolution in proceedings of the 5th international conference on Fluvial Hydraulics, Braunschweig, Germany.

[30] J. Hudson, P.K. Sweby. Formations for numerically approximating hyperbolic systems governing sediment transport. J. Scient. Comput. 19 (2003) 225-252.

[31] Alexender Kurganov, Finite volume schemes for shallow-water equations. Acta numerica; (2018), pp. 289-351.

[32] Kurganov and Tadmor, New high-resolution central-schemes for nonlinear conservation laws and convection-diffusion equations, J.Computer phys, 160(2000), pp. 241-282.

[33] P. Lax and B. Wendroff, Systems of conservation laws, Communications on Pure and Applied Mathematics, 13 (1960), pp. 217-237.

[34] LeVeque, R.J. Finite Volume Methods for Hyperbolic Problems. Cambridge University Press (2002), Cambridge, UK.

[35] Raphael Maurin, Julien Chauchat and Philippe Frey. Revisiting slope influence in turbulent bedload transport: consequences for vertical flow structure and transport rate scaling. Journal of Fluid Mechanics, Vol 839, 2018, pp. 135-156.

[36] Martinez-Aranda S., Murillo J. and Garcia-Navarro P, Comparison of new efficient 2D models for the simulation of bedload transport using the augmented Roe approach, Advances in Water Resources, July 2021.

[37] Sovanna Mean, Koichi Unami, Hisashi Okamoto, Masayuki Fujihara. A through description of one-dimensional steady open channel flows using the notion of viscosity solution. Applied mathematics and computation 415, (2022) 126730.

[38] Naveen Kumar Garg, G.D Veepapa Gowda. Godunov-type schemes for pressure less gas dynamics and related models. Applied Mathematics and Computation, vol 418, (2002),126790.

[39] R .W .D .Nickalls. A new bound for polynomials when all roots are real. The Mathematical Gazette, 95(534): pp. 520-526, November 2011. www.nickalls.org/dick/papers/maths/bounds2011.pdf.

[40] A .R .Ngatcha .N. Influence of physic and hydrodynamic parameters on uniform sediment transport formulas in a coastal and estuarine environment, Submited 2021.

[41] Boniface Nkonga and Praveen Chandrashekar. An exact Riemann solver for a shear shallow water model. In arxiv 19 Aout 2021.

[42] P .L .Roe, Upwinding difference schemes for hyperbolic conservation Laws with source terms, In Carasso, Raviart and Serre, editors, proceeding the conference on hyperbolic problems 41-51. Springer 1986.

[43] G .Rosatti and L .Fraccarolo. A well-balanced approach for flows over mobile-bed with high sediment transport. Journal of Computational Physics Volume 220, Issue 1, 20 December 2006, pp. 312-338. 7

[44] Soulsby RL, Whitehouse RJS, Marten KV. Prediction of time-evolving sand ripples in shelf seas. Continental Shelf Research(2012) (38):47-62.

[45] A .Siviglia, D .Vanzo, E .F .Toro, A splitting scheme for the coupled Saint-Venant-Exner model, Submited 2021.

[46] Soulsby RL, Whitehouse RJS, Marten KV. Prediction of time-evolving sand ripples in shelf seas. Continental Shelf Research(2012) (38):47-62.

[47] Toro, E., Vazquez-Cendon, M., 2012. Flux splitting schemes for the euler equations. Computers and Fluids 70, 1-12.

[48] Van Hieu Bui, Minh Duc Bui,and Peter Rutschmann. Advanced Numerical Modeling of Sediment Transport in Gravel-Bed Rivers. Water 2019, 11, 550; doi:10.3390/w11030550.

[49] VAH Mélanie, JARNO Armelle, MARIN François, LE BOT Sophie. Experimental Study on Sediment Supply-Limited Bedforms in a Coastal Context. Sixth International Conference on Estuaries and Coasts (ICEC-2018), August 20-23, 2018, Caen, France.

[50] Van Rijn LC. Equivalent roughness of alluvial bed. Journal of the Hydraulics Division (1982), 108(10): 1215-1218.

[51] A. I. Volpert, The spaces BV and quasilinear equations, Mathematics of the USSR-Sbornik, 2, 1967, pp. 225-267

[52] Weiming Wu and Sam .S .Wang, One-dimensional modeling of dam-break flow over movable beds, In journal of hydraulic engineering 133.1(2007), pp. 48-58. DOI 10.1061/(ASCE)0733-9429 (2007)133:1(48).

[53] Wilcock, P.R.; DeTemple, B.T. Persistence of armor layers in gravel-bed streams. Geophys. Res. Lett. 2005, 32.

[54] Xi Deng, Pierre Boivin, Feng Xiao. A new formulation for two-wave Riemann solver accurate at contact interfaces. Physics of Fluids, American Institute of Physics, 2019, 31 (4), pp.046102. 10.1063/1.5083888ff. hal-02100764ff.

[55] Xin Liu, Abdolmajid Mohammadian, Alexander Kurganov, Julio Angel Infante Sedano. Well-balanced central-upwind scheme for a fully coupled shallow water system modeling flows over erodible bed. Journal of Computational Physics 300 (2015) 202-218.